Arl13b regulates Sonic Hedgehog signaling from outside primary cilia

Eduardo D. Gigante[a,b], Megan R. Taylor[c], Anna A. Ivanova[d], Richard A. Kahn[d], Tamara Caspary[b]

[a]Neuroscience Graduate Program, [b]Department of Human Genetics, [c]Emory College of Arts and Sciences, [d]Department of Biochemistry, Emory University School of Medicine, Atlanta, GA 30322, USA

Author e-mails: Eduardo.gigante@emory.edu, meg.taylor@emory.edu, anna.ivanova@emory.edu, rkahn@emory.edu

ORCID ID: Gigante: 0000-0002-1486-5377, Kahn: 0000-0002-0259-0601, Caspary: 0000-0002-6579-7589

⌘**Correspondence**: Tamara Caspary

tcaspar@emory.edu

Abstract

ARL13B is a regulatory GTPase highly enriched in cilia. Complete loss of *Arl13b* disrupts cilia architecture, protein trafficking and Sonic hedgehog signaling. To determine whether ARL13B is required within cilia, we knocked in a cilia-excluded variant of ARL13B (V358A) and showed it retains all known biochemical function. We found that ARL13B^{V358A} protein was expressed but could not be detected in cilia, even when retrograde ciliary transport was blocked. We showed *Arl13b*$^{V358A/V358A}$ mice are viable and fertile with normal Shh signal transduction. However, in contrast to wild type cilia, *Arl13b*$^{V358A/V358A}$ cells displayed short cilia and lacked ciliary ARL3 and Inpp5e. These data indicate that ARL13B's role within cilia can be uncoupled from its function outside of cilia. Furthermore, these data imply that the cilia defects upon complete absence of ARL13B do not underlie the alterations in Shh transduction, which is unexpected given the requirement of cilia for Shh transduction.

Keywords:

ARL13B; Sonic Hedgehog signaling; primary cilia; mouse development

Introduction

13 The Hedgehog (Hh) signaling pathway is essential for embryogenesis in a wide
14 variety of organisms. Initially discovered in *Drosophila* where there is a single Hh ligand,
15 the core components of the Hh pathway are conserved in vertebrates (Nusslein-Volhard
16 and Wieschaus 1980). These include the vertebrate Hh receptor Patched1 (Ptch1), the
17 obligate transducer of the pathway Smoothened (Smo), as well as the Gli transcription
18 factors (Ci in *Drosophila*) that act as both activators (GliA) and repressors (GliR) to
19 control target gene transcription (Briscoe and Therond 2013). There are three Hh
20 ligands in vertebrates, Sonic (Shh), Indian (Ihh) and Desert (Dhh), that regulate a
21 multitude of developmental processes including formation of the limbs and digits, the
22 bones of the skull and face, and the patterning of the neural tube (Placzek and Briscoe
23 2018). Diminished Hh signaling during embryogenesis results in birth defects whereas
24 increased Hh signaling leads to tumors, highlighting the importance of the pathway and
25 its regulation (Raleigh and Reiter 2019).

26 Given the deep homology between invertebrate and vertebrate Hh signaling, the
27 discovery that primary cilia are required for vertebrate, but not invertebrate, Hh signaling
28 was unexpected (Huangfu et al. 2003; Huangfu and Anderson 2006). Vertebrate Hh
29 components dynamically traffic within cilia in response to ligand (Corbit et al. 2005;
30 Haycraft et al. 2005; Rohatgi et al. 2007). In the absence of ligand, Ptch1 is enriched on
31 the ciliary membrane and Smo is barely detectable (Corbit et al. 2005; Rohatgi et al.
32 2007). Furthermore, full length Gli proteins traffic to the ciliary tip and back to the
33 cytoplasm before being cleaved to their repressor form, which actively shuts down Hh
34 target gene transcription in the nucleus (Kim et al. 2009; Liu et al. 2005; Wen et al.

35 2010; Humke et al. 2010). In contrast, upon ligand stimulation (Shh, Ihh or Dhh), the
36 Ptch1 receptor binds the ligand and shuttles out of cilia (Rohatgi et al. 2007).
37 Subsequently, Smo is enriched in the cilium and is subsequently activated (Kong et al.
38 2019; Corbit et al. 2005). Activated Smo promotes the processing of full-length Gli
39 transcription factors into GliA, which turns on target genes (Aza-Blanc et al. 2000; Ruiz i
40 Altaba 1998). Ablation of cilia results in an absence of GliA and GliR production,
41 rendering the pathway inert and leading to an absence of transcriptional response
42 (Huangfu and Anderson 2005). The dynamic ciliary movement of Shh components
43 appears to be critical to pathway function, as alterations to cilia disrupt pathway output
44 (Caspary et al. 2007; Huangfu and Anderson 2006; Liem et al. 2012; Liem et al. 2009;
45 Goetz et al. 2009; Murdoch and Copp 2010; Tuz et al. 2014; Cortellino et al. 2009;
46 Houde et al. 2006; Liu et al. 2005; Tran et al. 2008; Taylor et al. 2015).
47 Given that the fundamental logic of the pathway is conserved from flies through
48 vertebrates, and that flies transduce Hh signals without relying on cilia, both
49 evolutionary and mechanistic questions are raised as to how vertebrate cells co-opted
50 the cilium for Hh signal transduction. One distinction lies in the fact that vertebrates use
51 Hh signaling over a longer distance than flies, leading to the proposal that the cilium is a
52 critical part of a mechanism underlying long range signaling (Bangs et al. 2015). For
53 example, in neural patterning Shh is initially expressed in the notochord and is secreted
54 to specify fates more than 20 cells away (Chiang et al. 1996; Briscoe et al. 2001;
55 Roelink et al. 1994). At the evolutionary level, comparisons among organisms with cilia
56 and or Hh have provided some clues. The round worm *C. elegans* have cilia yet do not
57 possess Hh signaling as they don't have most of the genes encoding the core

58 components of Hh signal transduction (Consortium 1998; Roy 2012). Curiously, a few
59 components of Hh signaling such as fused and costal 2 are in the *C. elegans* genome
60 where they are functionally important for ciliogenesis (Ingham et al. 2011). Additionally,
61 *C. elegans* retained a Ptch1 homolog important for development and pattern formation,
62 but no Hh or Smo (Zugasti et al. 2005; Kuwabara et al. 2000). In contrast, planaria
63 flatworms possess both cilia and Hh signaling but the cilia are not required to transduce
64 Hh signaling (Rink et al. 2009). These data suggest that the mechanistic link of cilia and
65 Hh is limited to vertebrates and originated in the last common ancestor of vertebrates,
66 the urochordates.

67 ARL13B is a member of the ARF family of regulatory GTPases and is highly
68 enriched on the ciliary membrane (Caspary et al. 2007). In mice, a null mutation of
69 *Arl13b* leads to short cilia and to alterations in Shh signal transduction (Caspary et al.
70 2007; Larkins et al. 2011). ARL13 is ancient, predicted to be present in the last common
71 eukaryotic ancestor. ARL13 appears to have been lost during evolution in organisms
72 that lack cilia and duplicated to ARL13A and ARL13B in the urochordates, thus ARL13B
73 is proposed to hold important clues in deciphering the links between cilia and vertebrate
74 Hh signaling (Schlacht et al. 2013; Li et al. 2004; Kahn et al. 2008; East et al. 2012;
75 Logsdon and Kahn 2004).

76 ARF regulatory GTPases, like ARL13B, are best known to play roles in
77 membrane trafficking (D'Souza-Schorey and Chavrier 2006). As is true for a large
78 number of regulatory GTPases, ARL13B is functionally diverse (Sztul et al. 2019). It
79 regulates endocytic traffic (Barral et al. 2012) as well as the phospholipid composition of
80 the ciliary membrane through recruitment of the lipid phosphatase Inpp5e to the ciliary

81 membrane (Humbert et al. 2012). ARL13B also has a conserved role as a guanine
82 nucleotide exchange factor (GEF) for ARL3, another ciliary ARF-like (ARL) protein
83 (Gotthardt et al. 2015; Zhang et al. 2016; Hanke-Gogokhia et al. 2016; Ivanova et al.
84 2017). ARL13B regulates intraflagellar transport (IFT), the process that builds and
85 maintains cilia (Cevik et al. 2010; Li et al. 2010; Nozaki et al. 2017). It is known to
86 interact with several proteins associated with cilia, including the exocyst, tubulin and
87 UNC119 (Seixas et al. 2016; Zhang et al. 2016; Larkins et al. 2011; Revenkova et al.
88 2018). Critical to this work, loss of ARL13B disrupts Shh signal transduction in at least
89 two distinct ways: Smo enrichment in cilia occurs even in the absence of ligand and Gli
90 activator production is diminished, although Gli repressor is made normally (Caspary et
91 al. 2007; Larkins et al. 2011).

92 Due to the high enrichment of ARL13B on the ciliary membrane, ARL13B is
93 assumed to function in its diverse roles from within the cilium. However, ARL13B is
94 present in early endosomes and circular dorsal ruffles on the cell surface (Barral et al.
95 2012; Casalou et al. 2014). We previously showed that a V358A variant of ARL13B
96 does not localize to cilia as it disrupts a known VxPx cilia localization sequence
97 (Higginbotham et al. 2012; Mariani et al. 2016). Exogenous overexpression of a
98 ARL13B^{V358A} construct in *Arl13b* null cells does not rescue ARL13B-dependent
99 phenotypes such as cilia length as well as interneuron migration and connectivity,
100 consistent with ciliary ARL13B mediating these processes (Higginbotham et al. 2012;
101 Mariani et al. 2016). In contrast, we found that overexpressed ARL13B^{V358A} does rescue
102 the Shh-dependent ciliary enrichment of Smo in mouse embryonic fibroblasts, arguing

103 that ARL13B may function outside the cilium to regulate Smo traffic (Mariani et al.
104 2016). Together, these results raise the question of where ARL13B functions.
105 To define where ARL13B functions in relation to cilia, we wanted an *in vivo*
106 model so generated mice carrying the ARL13B^{V358A} point mutation using CRISPR/Cas9.
107 Here we demonstrate that ARL13B^{V358A} protein was undetectable in *Arl13b*$^{V358A/V358A}$
108 cilia in both neural tube and mouse embryonic fibroblast cilia, even after blocking
109 retrograde ciliary traffic. We report that *Arl13b*$^{V358A/V358A}$ mice were viable, fertile, and
110 transduced Shh signal normally. We found ARL3 and Inpp5e did not localize to the
111 short cilia present in/on *Arl13b*$^{V358A/V358A}$ cells. These data indicate that ARL13B's roles
112 within and outside cilia can be uncoupled; ARL13B's role in regulating cilia length is
113 from within cilia, whereas its control of Shh signaling appears to be from outside the
114 cilium. Thus, these data imply that the cilia defects seen in the complete absence of
115 ARL13B do not underlie the alterations in Shh transduction, which is unexpected given
116 the requirement of cilia for Shh signal transduction.

Results

117 **ARL13B^{V358A} *displays normal GEF activity***

118 We previously showed that mouse ARL13B^{V358A} protein retained normal intrinsic
119 and GAP-stimulated GTP hydrolysis activities by analyzing GST-ARL13B^{V358A} purified
120 from human embryonic kidney (HEK) cells (Mariani et al. 2016). In order to test
121 ARL13B^{V358A} GEF activity for ARL3, we used the same GST-ARL13B^{V358A} protein
122 preparation and measured the rates of spontaneous or GEF-stimulated GDP
123 dissociation from ARL3 in the presence and absence of ARL13B or ARL13B^{V358A}. ARL3

124 spontaneously releases pre-bound GDP quite slowly under the conditions in the assay,
125 though release is linear with time, and by extrapolation requires just under 30 min for
126 50% of pre-bound [^{3}H]GDP to dissociate (**Figure 1**). In marked contrast, addition of
127 ARL13B under the same conditions caused the release of 50% of the GDP within ~10
128 seconds and close to 100% in one minute. We detected no differences between the wild
129 type and mutant ARL13B^{V358A} proteins in this assay, consistent with this point mutation
130 having no effect on ARL13B GEF function (**Figure 1**). This result is consistent with GEF
131 activity being conserved within the protein's GTPase domain while the V358A mutation
132 is located in the C-terminal domain (Gotthardt et al. 2015). These data indicate that
133 ARL13B^{V358A} retains all known ARL13B biochemical activities, suggesting that the
134 V358A mutation only disrupts ARL13B localization.
135
136 ***CRISPR engineered* Arl13b$^{V358A/V358A}$ *mice express cilia-excluded ARL13B protein.***
137 To determine the consequences of ARL13B^{V358A} expression *in vivo*, we used
138 CRISPR/Cas9 editing to change residue 358 from valine to alanine (**Figure 2A**). We
139 performed sequencing of the region that flanked exon 8, using primers outside the
140 region of the donor oligonucleotide. We confirmed the heterozygous T to C base pair
141 change for a valine to alanine change at residue 358 (**Figure 2B**). We backcrossed
142 heterozygous F1 progeny to FVB/NJ for three generations before analysis to minimize
143 any off target confounds (see details in Methods).
144 To determine whether ARL13B^{V358A} was detectable in neural tube cilia, we
145 performed immunofluorescence using antibodies directed against ARL13B and the cilia
146 marker IFT88. At embryonic day (E)10.5, we saw IFT88 staining, indicating the

147 presence of cilia. In neural tube cilia of *Arl13b*$^{+/+}$ and *Arl13b*$^{V358A/+}$ embryos, we
148 observed equivalent ARL13B staining but could not see ARL13B signal in neural tube
149 cilia of *Arl13b*$^{V358A/V358A}$ embryos, indicating the ARL13B^{V358A} protein is undetectable in
150 cilia *in vivo* (**Figure 2C**).

151 One possible explanation for the absence of ciliary ARL13B in the
152 *Arl13b*$^{V358A/V358A}$ embryos is that the ARL13B^{V358A} protein is not expressed or is
153 unstable. To determine whether ARL13B protein expression was affected by the V358A
154 mutation, we performed Western blots on E10.5 whole embryo lysates (**Figure 2D**). We
155 found a ~7% (±20%) reduction of ARL13B levels in *Arl13b*$^{V358A/+}$ embryos and a ~37%
156 (±6%) decrease of ARL13B levels in *Arl13b*$^{V358A/V358A}$ embryos, compared to WT
157 (**Figure 2E**). This decrease may reflect a change in ARL13B^{V358A} stability compared to
158 ciliary ARL13B or could signify ARL13B^{V358A} protein having a distinct half-life when
159 localizing to different cellular compartments. Regardless, these data indicate that
160 ARL13B^{V358A} is expressed in *Arl13b*$^{V358A/V358A}$ embryos.

161

162 ***ARL13B^{V358A} protein is undetectable in cilia in mouse embryonic fibroblasts.***

163 To more closely investigate whether any ARL13B^{V358A} protein could localize to
164 cilia, we generated immortalized mouse embryonic fibroblasts (MEFs). We performed
165 double labeling to first identify cilia using acetylated α-tubulin or IFT88 antibodies and
166 subsequently determined whether ARL13B is present in cilia. We used five distinct
167 antibodies against ARL13B: 4 antibodies against amino acids 208-427 of the mouse
168 ARL13B protein (1 mouse monoclonal (NeuroMab), 3 rabbit polyclonal antibodies
169 (Caspary et al. 2007)), as well as 1 antibody against the full-length human ARL13B

170 protein (rabbit polyclonal (Protein Tech)). By eye, we observed strong ciliary staining of
171 ARL13B with each of the antibodies in *Arl13b*$^{+/+}$ and *Arl13b*$^{V358A/+}$ cells, but we were
172 unable to identify any evidence of ARL13B staining above background within cilia in
173 *Arl13b*$^{V358A/V358A}$ cells with any of these five antibodies (**Figure 3A**). Taken together,
174 these data support our conclusion that ARL13B^{V358A} is not detectable in cilia using the
175 currently available, validated ARL13B antibodies.

176 While we observed no evidence of detectable ciliary ARL13B in *Arl13b*$^{V358A/V358A}$
177 MEFs, it is possible that a small amount of ARL13B^{V358A} is constantly trafficking in and
178 out of cilia, at steady-state levels that remain below the limits of detection. To address
179 this possibility, we blocked retrograde ciliary transport, reasoning that any ARL13B
180 undergoing trafficking in and out of cilia would accumulate. We treated cells with
181 ciliobrevin-D, which blocks the retrograde motor protein dynein (Firestone et al. 2012).
182 As a positive control, we examined IFT88, a ciliary protein known to accumulate at
183 ciliary tips upon blocking of retrograde transport. We found IFT88 enrichment at ciliary
184 tips in *Arl13b*$^{+/+}$, *Arl13b*$^{V358A/+}$ and *Arl13b*$^{V358A/V358A}$ cells upon ciliobrevin-D treatment
185 relative to the respective DMSO-treated controls with no difference in IFT88 staining
186 among the 3 genotypes (**Figure 3B**). To determine whether ARL13B accumulated in
187 cilia of ciliobrevin-D-treated MEFs, we examined cells co-stained for acetylated α-
188 tubulin and ARL13B. In *Arl13b*$^{+/+}$ and *Arl13b*$^{V358A/+}$ cells, we saw that about 90% of
189 acetylated α-tubulin-positive cilia also stained for ARL13B in DMSO-treated control or
190 ciliobrevin-D treated MEFs (**Figure 3C**). In *Arl13b*$^{V358A/V358A}$ MEFs, we saw no ciliary
191 ARL13B staining in DMSO-treated control or ciliobrevin-D-treated cells (**Figure 3C**).

192 Thus, even when retrograde traffic out of cilia is blocked, we were unable to detect
193 ARL13B protein in cilia in *Arl13b*$^{V358A/V358A}$ MEFs.
194 We re-examined these data and repeated our analyses using over-exposed
195 images. After defining the region of interest using the acetylated α-tubulin staining, we
196 subsequently overexposed the ARL13B channel five-fold relative to the images in
197 Figure 3 and acquired measurements at the cilium and the cell body (**Supplemental**
198 **Figure 1A**). As a control, we used *Arl13b*$^{hnn/hnn}$ MEFs, which are devoid of any ARL13B,
199 and obtained a ratio of 1.0, with or without ciliobrevin-D treatment. We found the same
200 ratio when we analyzed *Arl13b*$^{V358A/V358A}$ MEFs consistent with ARL13B being absent
201 from the cilia (**Supplemental Figure 1B, C**). We observed a few instances of ARL13B
202 appearing to co-localize with acetylated α-tubulin, but these were rare (<5%, 2/49) and
203 occurred in <u>both</u> *Arl13b*$^{V358A/V358A}$ and *Arl13b*$^{hnn/hnn}$ (null) cells indicating this is the
204 background staining of the primary antibody (**Supplemental Figure 1D**). We extended
205 our analysis of overexposed images in *Arl13b*$^{V358A/V358A}$ and *Arl13b*$^{hnn/hnn}$ neural tube
206 sections four-fold relative to the images in Figure 2; we identified no overlap of
207 overexposed ARL13B with cilia marker IFT88 (**Supplemental Figure 1E**). While it is
208 formally possible that an extremely small amount of ARL13B^{V358A} remains in cilia, we
209 are not able to find evidence of it; thus, we designate ARL13B^{V358A} protein as cilia-
210 excluded ARL13B.

Arl13b*$^{V358A/V358A}$ *mice are viable and fertile.

211 In order to determine the phenotypic consequence of the *Arl13b*^{V358A} allele, we
212 intercrossed *Arl13b*$^{V358A/+}$ mice. We observed progeny in Mendelian proportions with an

213 average of 7.3 pups per litter, consistent with the reported FVB/NJ litter size of 7-9
214 (Murray et al. 2010) (**Table 1**). To test whether homozygous mice breed normally, we
215 crossed *Arl13b*$^{V358A/V358A}$ males to heterozygous or homozygous females. We found the
216 *Arl13b*^{V358A} allele segregated in Mendelian proportions and the litter sizes were normal
217 indicating that *Arl13b*^{V358A} does not impact viability, fertility or fecundity.
218
219 ***ARL13B*^{V358A} *permits normal embryonic development and Shh signaling.***
220 Loss of *Arl13b* leads to morphologically abnormal embryos, lethality and neural
221 patterning defects (Caspary et al. 2007). As ARL13B^{V358A} overcame the embryonic
222 lethality, we examined overall embryo morphology at E9.5, E10.5 and E12.5. We found
223 the overall morphology of *Arl13b*$^{V358A/V358A}$ embryos resembled those of *Arl13b*$^{+/+}$ and
224 *Arl13b*$^{V358A/+}$ embryos indicating that ARL13B^{V358A} did not lead to gross morphological
225 defects. (**Figure 4A-I**).
226 At E9.5, Shh is normally expressed in the notochord as well as the floor plate of
227 the ventral neural tube. Moving dorsally, the adjacent domains express Nkx2.2 and
228 subsequently Olig2. In the *Arl13b*$^{hnn/hnn}$ (null) neural tube, the Shh-positive columnar
229 cells of the floor plate are absent resulting in both ventral and dorsal expansion of
230 intermediate Shh-dependent cell fates such as Olig2 (Caspary et al. 2007). To
231 determine whether ARL13B^{V358A} disrupts Shh signaling, we examined neural tube
232 patterning in *Arl13b*$^{+/+}$, *Arl13b*$^{V358A/+}$, and *Arl13b*$^{V358A/V358A}$ embryos at E9.5, E10.5, and
233 E12.5. At E9.5 we observed no differences in Shh, Nkx2.2 or Olig2 among *Arl13b*$^{+/+}$,
234 *Arl13b*$^{V358A/+}$, and *Arl13b*$^{V358A/V358A}$ embryos (**Figure 4A-C**). Cell fates in the neural tube
235 are specified by both the concentration and duration of Shh signaling so we examined

236 neural patterning at subsequent stages (Dessaud et al. 2007). By E10.5, some Olig2
237 precursors have differentiated to HB9+ motor neurons and all Shh-responsive cells
238 express Nkx6.1. We found that Olig2, HB9 and Nkx6.1 positive cells are normally
239 distributed in all 3 genotypes at E10.5 and E12.5 (**Figure 4D-I**). These data indicate that
240 ARL13B^{V358A} mediates normal Shh signaling.
241
242 ***ARL13B regulates ciliary enrichment of Shh components from outside cilia.***
243 In *Arl13b$^{hnn/hnn}$* cells, Smo is enriched in cilia in a Shh-independent manner,
244 which may be due to defective trafficking of Smo, as many ARL family members
245 regulate protein trafficking (Lim et al. 2011; Larkins et al. 2011). To assess Smo
246 enrichment in *Arl13b$^{V358A/V358A}$* embryos, we stained for the cilia marker acetylated α-
247 tubulin and Smo in E10.5 embryos. Smo appeared enriched normally in ventral floor
248 plate cilia and the dorsal boundary of Smo ciliary enrichment in ventral neural
249 progenitors was identical in *Arl13b$^{+/+}$*, *Arl13b$^{V358A/+}$*, and *Arl13b$^{V358A/V358A}$* samples
250 indicating ARL13B^{V358A} mediates normal ciliary Smo enrichment (**Figure 5A)**.
251 To examine Smo traffic in response to Shh stimulation, we treated MEFs with
252 0.5% FBS or Shh-conditioned media for 24 hours and stained for Smo. As expected in
253 control *Arl13b$^{hnn/hnn}$* cells, we saw ciliary Smo in unstimulated MEFs which increased
254 upon stimulation with Shh-conditioned media (Larkins et al. 2011) (**Figure 5B**). In
255 *Arl13b$^{+/+}$*, *Arl13b$^{V358A/+}$*, and *Arl13b$^{V358A/V358A}$* MEF cilia, we saw ciliary enrichment of
256 Smo upon Shh stimulation over their respective unstimulated controls (**Figure 5B**, left).
257 We found no difference in Smo enrichment among these cell lines (**Figure 5B**, right).
258 Thus, despite ARL13B being critical for Shh-dependent Smo ciliary enrichment,

259 ARL13B^{V358A} regulates Smo localization normally, arguing this function of ARL13B can
260 occur when the protein is not in cilia.
261 In addition to aberrations in Smo trafficking, loss of *Arl13b* leads to changes in
262 the cilia localization of other Shh components in MEFs (Larkins et al. 2011). To
263 determine whether these components are disrupted by ARL13B^{V358A}, we examined Gli2,
264 Gli3, Sufu and Ptch1 in MEFs. We observed no differences in distribution of Gli2 or
265 Ptch1 among any of the examined genotypes (**Figure 5C, F**). In contrast, as we
266 previously reported, we observed more Gli3 at the ciliary tip of *Arl13b$^{hnn/hnn}$* cells and
267 increased Sufu in *Arl13b$^{hnn/hnn}$* cilia compared to wild type controls (Larkins et al.
268 2011)(**Figure 5D, E**). Thus, Shh components are normally localized in *Arl13b$^{V358A/V358A}$*
269 MEFs consistent with the normal Shh signal transduction observed in *Arl13b$^{V358A/V358A}$*
270 embryos (**Figure 4**).
271
272 ***ARL13B regulates ciliary enrichment of ARL3 and Inpp5e from within cilia.***
273 We next examined the role of ARL13B^{V358A} in the localization of other ciliary
274 proteins. ARL13B is the GEF for ARL3, and we showed that ARL13B^{V358A} GEF activity
275 for ARL3 is normal (**Figure 1**). ARL13B is also essential for cilia localization of Inpp5e,
276 as the proteins are in a common complex (Humbert et al. 2012). To determine whether
277 the ciliary localization of either ARL3 or Inpp5e was affected by ARL13B^{V358A}, we
278 performed immunofluorescence on MEFs. Ciliary ARL3 staining appeared the same in
279 *Arl13b$^{+/+}$* and *Arl13b$^{V358A/+}$* MEFs, however ARL3 was not detectable in *Arl13b$^{V358A/V358A}$*
280 or *Arl13b$^{hnn/hnn}$* cilia (**Figure 5G**). Inpp5e was normally detectable in *Arl13b$^{+/+}$* and
281 *Arl13b$^{V358A/+}$* MEF cilia, but not in *Arl13b$^{V358A/V358A}$* and *Arl13b$^{hnn/hnn}$* MEF cilia (**Figure**

282 **5H**). These results indicate that ARL13B is required in cilia for the proper localization of
283 ARL3 and Inpp5e to the cilium.
284
285 ***Ciliary ARL13B is required for normal cell ciliation and ciliary length***
286 Loss of *Arl13b* leads to defects in the percentage of ciliated MEFs and in cilia
287 length (Caspary et al. 2007; Larkins et al. 2011). To test whether ARL13B^{V358A} impacted
288 cell ciliation, we examined immortalized MEFs and counted the number of ciliated cells
289 24 hours after induction of ciliation by growth in low serum (0.5% FBS). We found 73%
290 (±11%) of *Arl13b*$^{+/+}$ and 75%, (±9.1%) of *Arl13b*$^{V358A/+}$ MEFs are ciliated, consistent with
291 published results. In contrast, we found 45% (±8.7%) of *Arl13b*$^{V358A/V358A}$ cells and 53%
292 (±6.4%) of *Arl13b*$^{hnn/hnn}$ cells had cilia (**Figure 6A**). Thus, *Arl13b*$^{V358A/V358A}$ cells exhibit a
293 similar deficit in percentage of ciliated MEFs as complete loss of ARL13B function.
294 *Arl13b*$^{hnn/hnn}$ cilia are about half as long as wild type in both embryos and MEFs
295 (Caspary et al. 2007; Larkins et al. 2011). To determine whether cilia length was
296 affected by ARL13B^{V358A}, we stained MEFs with acetylated α–tubulin and measured the
297 length of the axoneme. We found the average cilia length in *Arl13b*$^{+/+}$ and Arl13b$^{V358A/+}$
298 MEFs was similar, 2.7 ± 0.8 μm and 2.6 ± 0.9 μm, respectively. However, we found
299 *Arl13b*$^{V358A/V358A}$ MEF cilia were shorter, 1.9 ± 0.7 μm, similar to *Arl13b*$^{hnn/hnn}$ MEF cilia
300 which were 2.15 ± 0.8 μm (**Figure 6B**). These results indicate that ARL13B^{V358A}
301 phenocopies complete loss of ARL13B for ciliation and cilia length, indicating these
302 ARL13B functions require ARL13B in cilia. Furthermore, these data show that ARL13B
303 function within cilia is distinct from ARL13B function outside of cilia in a subset of

304 activities, and that the cilia defects and Shh defects in the complete absence of ARL13B
305 can be uncoupled.

Discussion

306 Here we show that ARL13B's role(s) in cell ciliation and cilia length, along with
307 the ciliary enrichment of a subset of proteins, can be uncoupled from ARL13B's function
308 in regulating Shh signal transduction (**Figure 7**). Furthermore, we show this functional
309 distinction correlates with ARL13B spatial localization to the cilium. By generating a
310 mouse expressing a cilia-excluded variant of ARL13B from the endogenous locus, we
311 showed ARL13B^{V358A} protein is not detectable in cilia of embryonic neural tube or
312 MEFs, even upon retrograde ciliary traffic blockade. Furthermore, we detected 30% less
313 ARL13B protein overall in *Arl13b*$^{V358A/V358A}$ embryos compared to control embryos.
314 While this reduction is statistically significant, it is unclear whether it is biologically
315 significant given that *Arl13b*$^{hnn/hnn}$ null mutations are recessive and no *Arl13b*$^{hnn/+}$
316 heterozygous phenotype is reported (Caspary et al. 2007; Larkins et al. 2011).
317 In contrast to the E13.5 lethality of *Arl13b*$^{hnn/hnn}$ embryos, we found
318 *Arl13b*$^{V358A/V358A}$ mice were viable and fertile with correct patterning of the neural tube,
319 indicating normal Shh signal transduction. These results are consistent with our data
320 showing that ARL13B^{V358A} protein retains all known biochemical function including GEF
321 activity (Mariani et al. 2016; Ivanova et al. 2017). However, we observed several
322 *Arl13b*$^{hnn/hnn}$ phenotypes in *Arl13b*$^{V358A/V358A}$ cells, including loss of ARL3 and Inpp5e
323 ciliary enrichment, along with low percentage of ciliated cells and shorter average cilia
324 length. Taken together, our data show that despite the normal high ciliary enrichment of

325 wild type ARL13B and the requirement of cilia for Shh signaling, cilia-excluded
326 ARL13B^{V358A} is sufficient for Shh signal transduction.
327 We regard ARL13B^{V358A} as cilia-excluded based on several lines of evidence.
328 We did not detect ciliary ARL13B^{V358A} *in vivo* or *in vitro* using any of five validated
329 ARL13B antibodies. These antibodies are against two antigens, the full-length protein or
330 residues 208-427, and were independently generated so are likely to recognize a
331 number of epitopes. Given that 4 of 5 antibodies are polyclonal and ARL13B^{V358A}
332 displays normal GTP binding, intrinsic and GAP-stimulated GTP hydrolysis, and ARL3
333 GEF activity, it is likely that the ARL13B^{V358A} protein retains the wild type structure
334 enabling antibody recognition. Indeed, we observed little or no loss in sensitivity in
335 detecting protein in the immunoblot assays. Furthermore, we could not forcibly enrich
336 ciliary ARL13B^{V358A} through retrograde transport blockade with ciliobrevin-D nor could
337 we detect any ciliary enrichment of ARL13B^{V358A} upon overexposure of the relevant
338 fluorescent channel. The fact that we observed ciliary phenotypes, namely short cilia
339 and abnormal ciliary ARL3 and Inpp5e localization in ARL13B^{V358A} cells, argue that
340 ARL13B normally performs these functions from within cilia (Caspary et al. 2007;
341 Larkins et al. 2011; Zhang et al. 2016; Humbert et al. 2012; Nozaki et al. 2017). While
342 we cannot exclude the possibility that sub-detectable levels of ARL13B^{V358A} are present
343 and functional in cilia, we note such a level would need to be sufficient for Shh signaling
344 yet insufficient for ARL3 or Inpp5e ciliary localization along with proper regulation of cilia
345 length.
346 Our data support ARL13B regulating different biological processes from its
347 distinct subcellular localizations. ARL13B^{V358A} disrupts cilia localization of Inpp5e and

348 ARL3, but not Shh components. It is surprising that ARL13B^{V358A} is sufficient to regulate
349 Shh signaling because cilia are required for Shh signal transduction and because
350 ARL13B is highly enriched in cilia (Caspary et al. 2007; Huangfu et al. 2003). These
351 observations suggested that the ciliary defects observed in *Arl13b*$^{hnn/hnn}$ mutants caused
352 the Shh defects. However, our data with ARL13B^{V358A} indicate that ARL13B regulates
353 cilia length and Shh signaling through distinct localization and effectors.

354 Based on the normal cilia trafficking of Shh components in *ARL13B*$^{V358A/V358A}$
355 mutants and the abnormal cilia trafficking of Shh components in the complete absence
356 of ARL13B (Larkins et al. 2011), ARL13B likely regulates Shh signaling from the cell
357 body by controlling Shh component traffic to and/or from the cilium. Both Smo and
358 ARL13B traffic is linked to endosomes providing one possible non-ciliary organelle
359 (Barral et al. 2012; Wang et al. 2009; Milenkovic et al. 2009). *Arl13b*$^{hnn/hnn}$ cells display
360 constitutive Smo ciliary enrichment along with little enrichment of Gli proteins at the
361 ciliary tip (Larkins et al. 2011). Our data do not distinguish between ARL13B playing
362 direct roles in traffic of multiple Shh components or whether the normal Smo ciliary
363 enrichment with ARL13B^{V358A} subsequently causes normal cilia traffic of downstream
364 components. ARL13B regulates a step downstream of activated Smo that controls
365 transcription factor Gli activation, but not repression (Caspary et al. 2007; Bay et al.
366 2018). We argue from our results that this step is also intact in the presence of
367 ARL13B^{V358A}.

368 The fact that ARL13B^{V358A} can mediate normal ciliary Smo enrichment is
369 especially interesting given that ARL3 and Inpp5e localization to cilia is compromised by
370 this mutation. This suggests that ARL13B controls cilia enrichment via multiple

371 localizations and effectors. This is consistent with our understanding of ARF family
372 members, as they are known to perform multiple tasks from different sites within a cell
373 (Sztul et al. 2019). We speculate that ARL3 residence in cilia may require that ARL3 be
374 in (or at least cycle through) its activated, GTP-bound conformation as ARL13B^{V358A}
375 retains its ARL3 GEF activity, but not its cilia localization. ARL13B is in a common
376 protein complex with Inpp5e so absence of ARL13B from cilia may disrupt formation or
377 maintenance of the complex there (Humbert et al. 2012; Nozaki et al. 2017). Inpp5e
378 regulates Shh signaling through regulation of the phosphoinositol composition of the
379 ciliary membrane. Inpp5e loss results in increased ciliary PIP_2 and enrichment of Shh
380 repressors in cilia thus resulting in lowered Shh response (Garcia-Gonzalo et al. 2015;
381 Chavez et al. 2015; Dyson et al. 2017). It is not clear why the absence of ciliary Inpp5e
382 in ARL13B^{V358A} cells does not lead to aberrant Shh signal transduction.
383 In *Arl13b*$^{hnn/hnn}$ embryos and MEFs, cilia are shorter than normal and have a
384 microtubule defect where the B-tubule of the microtubule outer doublet is open
385 (Caspary et al. 2007; Larkins et al. 2011). Consistent with this, we observed shorter cilia
386 in *Arl13b*$^{V358A/V358A}$ MEFs. Similarly, we observed a comparable reduction in the percent
387 of cilia in *Arl13b*$^{hnn/hnn}$ and *Arl13b*$^{V358A/V358A}$ MEFs compared to wild type MEFs. While
388 loss of ARL13B results in short cilia, increased expression of ARL13B promotes cilia
389 elongation so it is not yet clear what ARL13B's role is in controlling cilia length (Lu et al.
390 2015; Hori et al. 2008; Caspary et al. 2007; Larkins et al. 2011). Additionally, it is
391 unclear whether the mechanism from within cilia through which ARL13B controls length
392 or percent of ciliated cells is the same, or distinct from, the mechanism through which
393 ARL13B regulates ARL3 or Inpp5e residence in cilia.

394 Perhaps the most intriguing implication of our data pertains to understanding the
395 evolution of cilia and Hh signaling. ARL13 functions in cilia formation and maintenance
396 in *Chlamydomonas* and *C. elegans*, neither of which have Hh signaling, consistent with
397 the ancient role of Arl13b controlling ciliation and cilia length (Cevik et al. 2010; Cevik et
398 al. 2013; Stolc et al. 2005; Miertzschke et al. 2014). Our data support ARL13B retaining
399 ARL13's ancient role in ciliogenesis. However, our data show that ARL13B does not
400 work from within the cilium to regulate Shh component ciliary traffic or Shh signal
401 transduction. As an ARL protein involved in membrane traffic, we speculate that
402 ARL13B may have linked Shh component trafficking to the cilium, albeit from outside
403 the cilium. That the ARL13 duplication in the urochordates coincides with when ARL13B
404 adopted new cellular roles in Hh signaling that linked the pathway to cilia fits well with
405 this model.

Methods

406 *Protein purification and ARL3 GEF assay*

407 Plasmids directing the expression of mouse GST-ARL13B or GST-ARL13B^{V358A}
408 proteins were transiently transfected into HEK cells and the recombinant proteins were
409 later purified by affinity chromatography using glutathione-Sepharose, as described
410 previously (Cavenagh et al. 1994; Ivanova et al. 2017). Human ARL3 (98.4% identical
411 to mouse ARL3) was expressed in BL21 bacteria and purified as previously described
412 (Van Valkenburgh et al. 2001). The ARL3 GEF assay was performed as previously
413 described (Ivanova et al. 2017). Briefly, ARL3 (10μM) was pre-incubated with [^{3}H]GDP
414 (1 μM; PerkinElmer Life Sciences, specific activity ~3,000 cpm/pmol) for 1 h at 30°C in

415 25 mM HEPES, pH 7.4, 100 mM NaCl, 10 mM $MgCl_2$. In contrast, pre-loading of
416 ARL13B (10μM) was achieved by incubation in 100 μM GTPγS for 1 min at room
417 temperature, due to its much more rapid exchange kinetics. The GEF assay was
418 initiated upon addition of ARL3 (final = 1μM), ARL13B (final = 0 or 1μM), 10 μM GTPγS,
419 and 100 μM GDP (to prevent re-binding of any released [^{3}H]GDP), in a final volume of
420 100 μL. The intrinsic rate of GDP dissociation from ARL3 was determined in parallel as
421 that released in the absence of any added ARL13B. The reactions were stopped at
422 different times (0–15 min) by dilution of 10μL of the reaction mixture into 2 ml of ice-cold
423 buffer (20 mM Tris, pH 7.5, 100 mM NaCl, 10 mM $MgCl_2$, 1 mM dithiothreitol). The
424 amount of ARL3-bound [^{3}H]GDP was determined by rapid filtration through BA85
425 nitrocellulose filters (0.45 μm, 25 mm, Whatman), with 3 x 2 mL washes, and quantified
426 using liquid scintillation counting. Time points are routinely collected in at least duplicate
427 and each experiment reported was repeated at least twice, yielding very similar results.
428 Data were analyzed in GraphPad Prism 7 software.
429
430 *Mouse allele generation and identification*
431 All mice were cared for in accordance with NIH guidelines and Emory's
432 Institutional Animal Care and Use Committee (IACUC). Lines used were *Arl13b*^{V358A}
433 (*Arl13b*^{em1Tc}) [MGI: 6256969], *Arl13b*^{hnn} [MGI: 3578151] and FVB/NJ (Jackson
434 Laboratory). To generate the V358A point mutation in the mouse, a CRISPR gRNA
435 (CCAGTCAATACAGACGAGTCTA) targeting exon 8 of the *Arl13b* locus along with a
436 donor oligo (5'-
437 CCTATATTCTTCTAGAAAACAGTAAGAAGAAAACCAAGAAACTACGAATGAAAAGGA

438 GTCATCGGGCAGAACCAGTGAATACAGACGAGTCTACTCCAAAGAGTCCCACGCC
439 TCCCCAAC-3'; underlined bases are engineered) were designed to generate a T-to-C
440 change creating the V358A point mutation and C-to-G change creating a TspRI
441 restriction site that could be used for genotyping (Millipore Sigma). The gRNA (50
442 ng/μl), oligo donor (50 ng/μl) and CRISPR protein (100 ng/μL) were injected by the
443 Emory Transgenic and Gene Targeting core into one-cell C57Bl/6J zygotes. Zygotes
444 were cultured to 2-cell before being transferred to pseudopregnant females. Genomic
445 tail DNA from resulting offspring was amplified using PCR primers (5'-
446 GAAGCAGGCATGGTGGTAAT-3' & 5'-TGAACCGCTAATGGGAAATC-3') located
447 upstream and downstream of the donor oligo breakpoints. The products were
448 sequenced (5'-GAAGCAGGCATGGTGGTAAT-3') and 2 animals were identified
449 heterozygous for the desired change and with no additional editing. One line (#173) was
450 bred to FVB/NJ for three generations prior to performing any phenotypic analysis. Males
451 from at least two distinct meiotic recombination opportunities were used in each
452 generation that to minimize potential confounds associated with off-target
453 CRISPR/Cas9 editing.
454 Genotyping was performed on DNA extracted from ear punch or yolk sac via
455 PCR using the following primers: Fwd: 5'- AAGAATGAAAAGGAGTCAGCG -3', Rev: 5'-
456 TGAACCGCTAATGGGAAACT -3'; a SNP was engineered in the forward primer that, in
457 combination with the V358A mutation, created a Cac8I restriction site. Thus, the PCR
458 product was digested with Cac8I enzyme, run out on a 4% agarose gel and the relevant
459 bands were detected: undigested wild type (~192bp) and digested mutant bands
460 (~171bp).

461

462 *Phenotypic analysis of embryos*

463 Timed matings of heterozygous intercrosses were performed to generate embryos of
464 the indicated stage, with somite-matched pairs examined at each stage when
465 appropriate. Embryos were dissected in cold phosphate-buffered saline and processed
466 for immunofluorescence staining? as previously described (Horner and Caspary 2011).

467

468 *Mouse embryonic fibroblasts*

469 Mouse embryonic fibroblasts (MEFs) were isolated and immortalized as previously
470 described (Mariani et al. 2016). MEFs were maintained in DMEM with 10% fetal bovine
471 serum (FBS) and 1% penicillin/streptomycin at 37°C in 5% CO_2. For experimental use,
472 *Arl13b*$^{+/+}$, *Arl13b*$^{V358A/+}$, and *Arl13b*$^{V358A/V358A}$ and *Arl13b*$^{hnn/hnn}$ MEFs were grown on
473 coverslips at a density of 0.5 x 10^6 cells/mL and treated for 24 h with 0.5% FBS Shh
474 conditioned media or 0.5% FBS media to induce ciliogenesis (Larkins et al. 2011).

475

476 *Antibodies*

477 Primary antibodies used were: mouse anti-Shh (5E1), mouse anti-Nkx2.2 (74.5A5),
478 mouse anti-HB9 (81.5C10) (1:5 Developmental Studies Hybridoma Bank); rabbit anti-
479 Olig2 (1:300 Millipore AB9610); mouse anti-acetylated α-tubulin (1:2500 Millipore
480 Sigma; T6793), mouse anti-Arl13b (1:1000 NeuroMab N295B/66), rabbit anti-Arl13b
481 (1:1000, Protein Tech 17711-1-AP); rabbit anti-Arl13b sera from 3 distinct rabbits (503,
482 504 and 505) (Caspary Lab (Caspary et al. 2007)), rabbit anti-Smoothened (1:1000,
483 kindly provided by K. Anderson); rabbit anti-IFT88 (1:1000, kindly provided by B.

484 Yoder); rabbit anti-ARL3 (1:1000, (Cavenagh et al. 1994)); rabbit anti-Inpp5e (1:150,
485 Protein Tech 17797-1-AP); guinea pig anti-Gli2 (1:200, kindly provided by J.
486 Eggenschwiler); rabbit anti-Ptch1 (1:150, kindly provided by R. Rohatgi), goat anti-Sufu
487 (1:100, SC10933, Santa Cruz); goat anti-Gli3 (1:200, R&D AF3690) Alexa Fluor 488
488 and Alexa Fluor 568 (1:300, ThermoFisher); and Hoechst nuclear stain (1:3000).
489
490 *Image Quantification*
491 Fluorescent intensities were measured in ImageJ software. Cilia were first identified by
492 positive acetylated α-tubulin and an outline was hand drawn around the length of the
493 cilium. The channel was switched to the protein of interest and a measurement of the
494 average fluorescent intensity was acquired. The same outline was then used to acquire
495 a background reading of the cell-body that most closely matched the background at the
496 cilium. In all cases immunofluorescent averages of proteins of interest in cilia were
497 normalized to cell-body intensities (Supplemental Figure 1A). For samples with
498 antibodies targeting Gli2, Gli3, and Sufu the ciliary tip was isolated and measured. The
499 cilia tip was identified by weak acetylated α-tubulin staining or the cilium base was
500 identified by the presence of the acetylated α-tubulin positive fibrils in the cell body that
501 cluster at the base of the cilium (Larkins et al. 2011). For samples with antibodies
502 targeting Smo, Ptch1, ARL3, and Inpp5e the entire cilium was measured. We plotted
503 the ratio of fluorescence intensity of the protein of interest to the cell body background.
504 The number of cilia examined per genotype and per condition are listed below their
505 respective violin plot. Data were analyzed by one-way ANOVA, except for Smo intensity
506 where a two-way ANOVA was used with Sidak's multiple comparison. In the event of a

507 significant ANOVA, Tukey's multiple comparisons were employed to determine
508 significance. Data were analyzed in GraphPad Prism 7 software.
509 In a similar experiment, retrograde IFT was inhibited by the addition of 30 μM
510 ciliobrevin-D (Millipore Sigma; 250401) or 0.1% DMSO control in low-serum media for
511 60 min after ciliation was induced by serum starvation for 24 h prior with 0.5% FBS
512 media. Cilia were identified by staining with antibodies directed against acetylated α-
513 tubulin, IFT88, and ARL13B. Fluorescent intensities were measured in ImageJ software.
514 Again, cilia were first identified by positive acetylated α-tubulin and an outline was hand
515 drawn. The channel was switched to the protein of interest and a measurement of the
516 average fluorescent intensity was acquired. The same outline was then used to acquire
517 a background reading of the cell-body. To measure IFT88, the cilia tip was identified by
518 weak acetylated α-tubulin staining or the cilium base was identified by the presence of
519 acetylated α-tubulin fibrils in the cell body that cluster at the base of the cilium (Larkins
520 et al. 2011). Data were analyzed by two-way ANOVA with Sidak's multiple comparison.
521
522 *Western Blots*
523 Western blotting was performed as previously described (Mariani et al. 2016), with
524 antibody against ARL13B (1:1000 Neuromab N295B/66). Lysates were prepared with
525 RIPA buffer and SigmaFast protease inhibitors (Nachtergaele et al. 2013). Values
526 presented as volume intensity measured by chemiluminescence detected on ChemiDoc
527 Touch Imaging System were normalized to total protein as measured on a stain-free
528 gel. Normalized values were analyzed by one-way ANOVA and Tukey's multiple
529 comparisons. Data were analyzed in GraphPad Prism 7 software.

Acknowledgements

This work was supported by funding from NIH grants R01NS090029 and R35GM122549 to T.C. and R35GM122568 to R.A.K. E.D.G. was supported by R01NS090029 diversity supplement. Further support came from the Emory Integrated Mouse Transgenic and Gene Targeting Core, which is subsidized by the Emory University School of Medicine and with support by the Georgia Clinical & Translational Science Alliance of the National Institutes of Health under Award Number UL1TR002378 as well as the Emory University Integrated Cellular Imaging Microscopy Core of the Emory Neuroscience NINDS Core Facilities grant, P30NS055077. We are grateful to Alyssa Long and Sarah Suciu for sequencing potential CRISPR founders, and to members of the Caspary lab for discussion and manuscript comments.

Competing Interests

The authors have no competing interests to disclose.

References

542 Aza-Blanc, P., H. Y. Lin, A. Ruiz i Altaba, and T. B. Kornberg. 2000. 'Expression of the
543 vertebrate Gli proteins in Drosophila reveals a distribution of activator and repressor
544 activities', *Development*, 127: 4293-301.
545 Bangs, F. K., N. Schrode, A. K. Hadjantonakis, and K. V. Anderson. 2015. 'Lineage specificity of
546 primary cilia in the mouse embryo', *Nat Cell Biol*, 17: 113-22.
547 Barral, D. C., S. Garg, C. Casalou, G. F. Watts, J. L. Sandoval, J. S. Ramalho, V. W. Hsu, and
548 M. B. Brenner. 2012. 'Arl13b regulates endocytic recycling traffic', *Proc Natl Acad Sci U*
549 *S A*, 109: 21354-9.
550 Bay, S. N., A. B. Long, and T. Caspary. 2018. 'Disruption of the ciliary GTPase Arl13b
551 suppresses Sonic hedgehog overactivation and inhibits medulloblastoma formation',
552 *Proc Natl Acad Sci U S A*, 115: 1570-75.
553 Briscoe, J., Y. Chen, T. M. Jessell, and G. Struhl. 2001. 'A hedgehog-insensitive form of
554 patched provides evidence for direct long-range morphogen activity of sonic hedgehog
555 in the neural tube', *Mol Cell*, 7: 1279-91.
556 Briscoe, J., and P. P. Therond. 2013. 'The mechanisms of Hedgehog signalling and its roles in
557 development and disease', *Nat Rev Mol Cell Biol*, 14: 416-29.
558 Casalou, C., C. Seixas, A. Portelinha, P. Pintado, M. Barros, J. S. Ramalho, S. S. Lopes, and D.
559 C. Barral. 2014. 'Arl13b and the non-muscle myosin heavy chain IIA are required for
560 circular dorsal ruffle formation and cell migration', *J Cell Sci*, 127: 2709-22.
561 Caspary, T., C. E. Larkins, and K. V. Anderson. 2007. 'The graded response to Sonic Hedgehog
562 depends on cilia architecture', *Dev Cell*, 12: 767-78.
563 Cavenagh, M. M., M. Breiner, A. Schurmann, A. G. Rosenwald, T. Terui, C. Zhang, P. A.
564 Randazzo, M. Adams, H. G. Joost, and R. A. Kahn. 1994. 'ADP-ribosylation factor
565 (ARF)-like 3, a new member of the ARF family of GTP-binding proteins cloned from
566 human and rat tissues', *J Biol Chem*, 269: 18937-42.
567 Cevik, S., Y. Hori, O. I. Kaplan, K. Kida, T. Toivenon, C. Foley-Fisher, D. Cottell, T. Katada, K.
568 Kontani, and O. E. Blacque. 2010. 'Joubert syndrome Arl13b functions at ciliary
569 membranes and stabilizes protein transport in Caenorhabditis elegans', *J Cell Biol*, 188:
570 953-69.
571 Cevik, S., A. A. Sanders, E. Van Wijk, K. Boldt, L. Clarke, J. van Reeuwijk, Y. Hori, N. Horn, L.
572 Hetterschijt, A. Wdowicz, A. Mullins, K. Kida, O. I. Kaplan, S. E. van Beersum, K. Man
573 Wu, S. J. Letteboer, D. A. Mans, T. Katada, K. Kontani, M. Ueffing, R. Roepman, H.
574 Kremer, and O. E. Blacque. 2013. 'Active transport and diffusion barriers restrict Joubert
575 Syndrome-associated ARL13B/ARL-13 to an Inv-like ciliary membrane subdomain',
576 *PLoS Genet*, 9: e1003977.
577 Chavez, M., S. Ena, J. Van Sande, A. de Kerchove d'Exaerde, S. Schurmans, and S. N.
578 Schiffmann. 2015. 'Modulation of Ciliary Phosphoinositide Content Regulates Trafficking
579 and Sonic Hedgehog Signaling Output', *Dev Cell*, 34: 338-50.
580 Chiang, C., Y. Litingtung, E. Lee, K. E. Young, J. L. Corden, H. Westphal, and P. A. Beachy.
581 1996. 'Cyclopia and defective axial patterning in mice lacking Sonic hedgehog gene
582 function', *Nature*, 383: 407-13.
583 Consortium, C. elegans Sequencing. 1998. 'Genome sequence of the nematode C. elegans: a
584 platform for investigating biology', *Science*, 282: 2012-8.
585 Corbit, K. C., P. Aanstad, V. Singla, A. R. Norman, D. Y. Stainier, and J. F. Reiter. 2005.
586 'Vertebrate Smoothened functions at the primary cilium', *Nature*, 437: 1018-21.
587 Cortellino, S., C. Wang, B. Wang, M. R. Bassi, E. Caretti, D. Champeval, A. Calmont, M. Jarnik,
588 J. Burch, K. S. Zaret, L. Larue, and A. Bellacosa. 2009. 'Defective ciliogenesis,
589 embryonic lethality and severe impairment of the Sonic Hedgehog pathway caused by

590 inactivation of the mouse complex A intraflagellar transport gene Ift122/Wdr10, partially
591 overlapping with the DNA repair gene Med1/Mbd4', *Dev Biol*, 325: 225-37.
592 D'Souza-Schorey, C., and P. Chavrier. 2006. 'ARF proteins: roles in membrane traffic and
593 beyond', *Nat Rev Mol Cell Biol*, 7: 347-58.
594 Dessaud, E., L. L. Yang, K. Hill, B. Cox, F. Ulloa, A. Ribeiro, A. Mynett, B. G. Novitch, and J.
595 Briscoe. 2007. 'Interpretation of the sonic hedgehog morphogen gradient by a temporal
596 adaptation mechanism', *Nature*, 450: 717-20.
597 Dyson, J. M., S. E. Conduit, S. J. Feeney, S. Hakim, T. DiTommaso, A. J. Fulcher, A. Sriratana,
598 G. Ramm, K. A. Horan, R. Gurung, C. Wicking, I. Smyth, and C. A. Mitchell. 2017.
599 'INPP5E regulates phosphoinositide-dependent cilia transition zone function', *J Cell Biol*,
600 216: 247-63.
601 East, M. P., J. B. Bowzard, J. B. Dacks, and R. A. Kahn. 2012. 'ELMO domains, evolutionary
602 and functional characterization of a novel GTPase-activating protein (GAP) domain for
603 Arf protein family GTPases', *J Biol Chem*, 287: 39538-53.
604 Firestone, A. J., J. S. Weinger, M. Maldonado, K. Barlan, L. D. Langston, M. O'Donnell, V. I.
605 Gelfand, T. M. Kapoor, and J. K. Chen. 2012. 'Small-molecule inhibitors of the AAA+
606 ATPase motor cytoplasmic dynein', *Nature*, 484: 125-9.
607 Garcia-Gonzalo, F. R., S. C. Phua, E. C. Roberson, G. Garcia, 3rd, M. Abedin, S. Schurmans,
608 T. Inoue, and J. F. Reiter. 2015. 'Phosphoinositides Regulate Ciliary Protein Trafficking
609 to Modulate Hedgehog Signaling', *Dev Cell*, 34: 400-09.
610 Goetz, S. C., P. J. Ocbina, and K. V. Anderson. 2009. 'The primary cilium as a Hedgehog signal
611 transduction machine', *Methods Cell Biol*, 94: 199-222.
612 Gotthardt, K., M. Lokaj, C. Koerner, N. Falk, A. Giessl, and A. Wittinghofer. 2015. 'A G-protein
613 activation cascade from Arl13B to Arl3 and implications for ciliary targeting of lipidated
614 proteins', *Elife*, 4.
615 Hanke-Gogokhia, C., Z. Wu, C. D. Gerstner, J. M. Frederick, H. Zhang, and W. Baehr. 2016.
616 'Arf-like Protein 3 (ARL3) Regulates Protein Trafficking and Ciliogenesis in Mouse
617 Photoreceptors', *J Biol Chem*, 291: 7142-55.
618 Haycraft, C. J., B. Banizs, Y. Aydin-Son, Q. Zhang, E. J. Michaud, and B. K. Yoder. 2005. 'Gli2
619 and Gli3 localize to cilia and require the intraflagellar transport protein polaris for
620 processing and function', *PLoS Genet*, 1: e53.
621 Higginbotham, H., T. Y. Eom, L. E. Mariani, A. Bachleda, J. Hirt, V. Gukassyan, C. L. Cusack,
622 C. Lai, T. Caspary, and E. S. Anton. 2012. 'Arl13b in primary cilia regulates the migration
623 and placement of interneurons in the developing cerebral cortex', *Dev Cell*, 23: 925-38.
624 Hori, Y., T. Kobayashi, Y. Kikko, K. Kontani, and T. Katada. 2008. 'Domain architecture of the
625 atypical Arf-family GTPase Arl13b involved in cilia formation', *Biochem Biophys Res*
626 *Commun*, 373: 119-24.
627 Horner, V. L., and T. Caspary. 2011. 'Disrupted dorsal neural tube BMP signaling in the cilia
628 mutant Arl13b hnn stems from abnormal Shh signaling', *Dev Biol*, 355: 43-54.
629 Houde, C., R. J. Dickinson, V. M. Houtzager, R. Cullum, R. Montpetit, M. Metzler, E. M.
630 Simpson, S. Roy, M. R. Hayden, P. A. Hoodless, and D. W. Nicholson. 2006. 'Hippi is
631 essential for node cilia assembly and Sonic hedgehog signaling', *Dev Biol*, 300: 523-33.
632 Huangfu, D., and K. V. Anderson. 2005. 'Cilia and Hedgehog responsiveness in the mouse',
633 *Proc Natl Acad Sci U S A*, 102: 11325-30.
634 ———. 2006. 'Signaling from Smo to Ci/Gli: conservation and divergence of Hedgehog
635 pathways from Drosophila to vertebrates', *Development*, 133: 3-14.
636 Huangfu, D., A. Liu, A. S. Rakeman, N. S. Murcia, L. Niswander, and K. V. Anderson. 2003.
637 'Hedgehog signalling in the mouse requires intraflagellar transport proteins', *Nature*, 426:
638 83-7.

639 Humbert, M. C., K. Weihbrecht, C. C. Searby, Y. Li, R. M. Pope, V. C. Sheffield, and S. Seo.
640 2012. 'ARL13B, PDE6D, and CEP164 form a functional network for INPP5E ciliary
641 targeting', *Proc Natl Acad Sci U S A*, 109: 19691-6.
642 Humke, E. W., K. V. Dorn, L. Milenkovic, M. P. Scott, and R. Rohatgi. 2010. 'The output of
643 Hedgehog signaling is controlled by the dynamic association between Suppressor of
644 Fused and the Gli proteins', *Genes Dev*, 24: 670-82.
645 Ingham, P. W., Y. Nakano, and C. Seger. 2011. 'Mechanisms and functions of Hedgehog
646 signalling across the metazoa', *Nat Rev Genet*, 12: 393-406.
647 Ivanova, A. A., T. Caspary, N. T. Seyfried, D. M. Duong, A. B. West, Z. Liu, and R. A. Kahn.
648 2017. 'Biochemical characterization of purified mammalian ARL13B protein indicates
649 that it is an atypical GTPase and ARL3 guanine nucleotide exchange factor (GEF)', *J*
650 *Biol Chem*, 292: 11091-108.
651 Kahn, R. A., E. Bruford, H. Inoue, J. M. Logsdon, Jr., Z. Nie, R. T. Premont, P. A. Randazzo, M.
652 Satake, A. B. Theibert, M. L. Zapp, and D. Cassel. 2008. 'Consensus nomenclature for
653 the human ArfGAP domain-containing proteins', *J Cell Biol*, 182: 1039-44.
654 Kim, J., M. Kato, and P. A. Beachy. 2009. 'Gli2 trafficking links Hedgehog-dependent activation
655 of Smoothened in the primary cilium to transcriptional activation in the nucleus', *Proc*
656 *Natl Acad Sci U S A*, 106: 21666-71.
657 Kong, J. H., C. Siebold, and R. Rohatgi. 2019. 'Biochemical mechanisms of vertebrate
658 hedgehog signaling', *Development*, 146.
659 Kuwabara, P. E., M. H. Lee, T. Schedl, and G. S. Jefferis. 2000. 'A C. elegans patched gene,
660 ptc-1, functions in germ-line cytokinesis', *Genes Dev*, 14: 1933-44.
661 Larkins, C. E., G. D. Aviles, M. P. East, R. A. Kahn, and T. Caspary. 2011. 'Arl13b regulates
662 ciliogenesis and the dynamic localization of Shh signaling proteins', *Mol Biol Cell*, 22:
663 4694-703.
664 Li, Y., W. G. Kelly, J. M. Logsdon, Jr., A. M. Schurko, B. D. Harfe, K. L. Hill-Harfe, and R. A.
665 Kahn. 2004. 'Functional genomic analysis of the ADP-ribosylation factor family of
666 GTPases: phylogeny among diverse eukaryotes and function in C. elegans', *FASEB J*,
667 18: 1834-50.
668 Li, Y., Q. Wei, Y. Zhang, K. Ling, and J. Hu. 2010. 'The small GTPases ARL-13 and ARL-3
669 coordinate intraflagellar transport and ciliogenesis', *J Cell Biol*, 189: 1039-51.
670 Liem, K. F., Jr., A. Ashe, M. He, P. Satir, J. Moran, D. Beier, C. Wicking, and K. V. Anderson.
671 2012. 'The IFT-A complex regulates Shh signaling through cilia structure and membrane
672 protein trafficking', *J Cell Biol*, 197: 789-800.
673 Liem, K. F., Jr., M. He, P. J. Ocbina, and K. V. Anderson. 2009. 'Mouse Kif7/Costal2 is a cilia-
674 associated protein that regulates Sonic hedgehog signaling', *Proc Natl Acad Sci U S A*,
675 106: 13377-82.
676 Lim, Y. S., C. E. Chua, and B. L. Tang. 2011. 'Rabs and other small GTPases in ciliary
677 transport', *Biol Cell*, 103: 209-21.
678 Liu, A., B. Wang, and L. A. Niswander. 2005. 'Mouse intraflagellar transport proteins regulate
679 both the activator and repressor functions of Gli transcription factors', *Development*, 132:
680 3103-11.
681 Logsdon, J. M., Jr., and R. A. Kahn (ed.)^(eds.). 2004. *Arf Family GTPases. In: Kahn RA, editor.*
682 Lu, H., M. T. Toh, V. Narasimhan, S. K. Thamilselvam, S. P. Choksi, and S. Roy. 2015. 'A
683 function for the Joubert syndrome protein Arl13b in ciliary membrane extension and
684 ciliary length regulation', *Dev Biol*, 397: 225-36.
685 Mariani, L. E., M. F. Bijlsma, A. I. Ivanova, S. K. Suciu, R. A. Kahn, and T. Caspary. 2016.
686 'Arl13b regulates Shh signaling from both inside and outside the cilium', *Mol Biol Cell*.
687 Miertzschke, M., C. Koerner, M. Spoerner, and A. Wittinghofer. 2014. 'Structural insights into the
688 small G-protein Arl13B and implications for Joubert syndrome', *Biochem J*, 457: 301-11.

689 Milenkovic, L., M. P. Scott, and R. Rohatgi. 2009. 'Lateral transport of Smoothened from the
690 plasma membrane to the membrane of the cilium', *J Cell Biol*, 187: 365-74.
691 Murdoch, J. N., and A. J. Copp. 2010. 'The relationship between sonic Hedgehog signaling,
692 cilia, and neural tube defects', *Birth Defects Res A Clin Mol Teratol*, 88: 633-52.
693 Murray, S. A., J. L. Morgan, C. Kane, Y. Sharma, C. S. Heffner, J. Lake, and L. R. Donahue.
694 2010. 'Mouse gestation length is genetically determined', *PLoS One*, 5: e12418.
695 Nachtergaele, S., D. M. Whalen, L. K. Mydock, Z. Zhao, T. Malinauskas, K. Krishnan, P. W.
696 Ingham, D. F. Covey, C. Siebold, and R. Rohatgi. 2013. 'Structure and function of the
697 Smoothened extracellular domain in vertebrate Hedgehog signaling', *Elife*, 2: e01340.
698 Nozaki, S., Y. Katoh, M. Terada, S. Michisaka, T. Funabashi, S. Takahashi, K. Kontani, and K.
699 Nakayama. 2017. 'Regulation of ciliary retrograde protein trafficking by the Joubert
700 syndrome proteins ARL13B and INPP5E', *J Cell Sci*, 130: 563-76.
701 Nusslein-Volhard, C., and E. Wieschaus. 1980. 'Mutations affecting segment number and
702 polarity in Drosophila', *Nature*, 287: 795-801.
703 Placzek, M., and J. Briscoe. 2018. 'Sonic hedgehog in vertebrate neural tube development', *Int*
704 *J Dev Biol*, 62: 225-34.
705 Raleigh, D. R., and J. F. Reiter. 2019. 'Misactivation of Hedgehog signaling causes inherited
706 and sporadic cancers', *J Clin Invest*, 129: 465-75.
707 Revenkova, E., Q. Liu, G. L. Gusella, and C. Iomini. 2018. 'The Joubert syndrome protein
708 ARL13B binds tubulin to maintain uniform distribution of proteins along the ciliary
709 membrane', *J Cell Sci*, 131.
710 Rink, J. C., K. A. Gurley, S. A. Elliott, and A. Sanchez Alvarado. 2009. 'Planarian Hh signaling
711 regulates regeneration polarity and links Hh pathway evolution to cilia', *Science*, 326:
712 1406-10.
713 Roelink, H., A. Augsburger, J. Heemskerk, V. Korzh, S. Norlin, A. Ruiz i Altaba, Y. Tanabe, M.
714 Placzek, T. Edlund, T. M. Jessell, and et al. 1994. 'Floor plate and motor neuron
715 induction by vhh-1, a vertebrate homolog of hedgehog expressed by the notochord',
716 *Cell*, 76: 761-75.
717 Rohatgi, R., L. Milenkovic, and M. P. Scott. 2007. 'Patched1 regulates hedgehog signaling at
718 the primary cilium', *Science*, 317: 372-6.
719 Roy, S. 2012. 'Cilia and Hedgehog: when and how was their marriage solemnized?',
720 *Differentiation*, 83: S43-8.
721 Ruiz i Altaba, A. 1998. 'Combinatorial Gli gene function in floor plate and neuronal inductions by
722 Sonic hedgehog', *Development*, 125: 2203-12.
723 Schlacht, A., K. Mowbrey, M. Elias, R. A. Kahn, and J. B. Dacks. 2013. 'Ancient complexity,
724 opisthokont plasticity, and discovery of the 11th subfamily of Arf GAP proteins', *Traffic*,
725 14: 636-49.
726 Seixas, C., S. Y. Choi, N. Polgar, N. L. Umberger, M. P. East, X. Zuo, H. Moreiras, R.
727 Ghossoub, A. Benmerah, R. A. Kahn, B. Fogelgren, T. Caspary, J. H. Lipschutz, and D.
728 C. Barral. 2016. 'Arl13b and the exocyst interact synergistically in ciliogenesis', *Mol Biol*
729 *Cell*, 27: 308-20.
730 Stolc, V., M. P. Samanta, W. Tongprasit, and W. F. Marshall. 2005. 'Genome-wide
731 transcriptional analysis of flagellar regeneration in Chlamydomonas reinhardtii identifies
732 orthologs of ciliary disease genes', *Proc Natl Acad Sci U S A*, 102: 3703-7.
733 Sztul, E., P. W. Chen, J. E. Casanova, J. Cherfils, J. B. Dacks, D. G. Lambright, F. S. Lee, P. A.
734 Randazzo, L. C. Santy, A. Schurmann, I. Wilhelmi, M. E. Yohe, and R. A. Kahn. 2019.
735 'ARF GTPases and their GEFs and GAPs: concepts and challenges', *Mol Biol Cell*, 30:
736 1249-71.
737 Taylor, S. P., T. J. Dantas, I. Duran, S. Wu, R. S. Lachman, Consortium University of
738 Washington Center for Mendelian Genomics, S. F. Nelson, D. H. Cohn, R. B. Vallee,

739 and D. Krakow. 2015. 'Mutations in DYNC2LI1 disrupt cilia function and cause short rib
740 polydactyly syndrome', *Nat Commun*, 6: 7092.
741 Tran, P. V., C. J. Haycraft, T. Y. Besschetnova, A. Turbe-Doan, R. W. Stottmann, B. J. Herron,
742 A. L. Chesebro, H. Qiu, P. J. Scherz, J. V. Shah, B. K. Yoder, and D. R. Beier. 2008.
743 'THM1 negatively modulates mouse sonic hedgehog signal transduction and affects
744 retrograde intraflagellar transport in cilia', *Nat Genet*, 40: 403-10.
745 Tuz, K., R. Bachmann-Gagescu, D. R. O'Day, K. Hua, C. R. Isabella, I. G. Phelps, A. E.
746 Stolarski, B. J. O'Roak, J. C. Dempsey, C. Lourenco, A. Alswaid, C. G. Bonnemann, L.
747 Medne, S. Nampoothiri, Z. Stark, R. J. Leventer, M. Topcu, A. Cansu, S. Jagadeesh, S.
748 Done, G. E. Ishak, I. A. Glass, J. Shendure, S. C. Neuhauss, C. R. Haldeman-Englert,
749 D. Doherty, and R. J. Ferland. 2014. 'Mutations in CSPP1 cause primary cilia
750 abnormalities and Joubert syndrome with or without Jeune asphyxiating thoracic
751 dystrophy', *Am J Hum Genet*, 94: 62-72.
752 Van Valkenburgh, H., J. F. Shern, J. D. Sharer, X. Zhu, and R. A. Kahn. 2001. 'ADP-ribosylation
753 factors (ARFs) and ARF-like 1 (ARL1) have both specific and shared effectors:
754 characterizing ARL1-binding proteins', *J Biol Chem*, 276: 22826-37.
755 Wang, Y., Z. Zhou, C. T. Walsh, and A. P. McMahon. 2009. 'Selective translocation of
756 intracellular Smoothened to the primary cilium in response to Hedgehog pathway
757 modulation', *Proc Natl Acad Sci U S A*, 106: 2623-8.
758 Wen, X., C. K. Lai, M. Evangelista, J. A. Hongo, F. J. de Sauvage, and S. J. Scales. 2010.
759 'Kinetics of hedgehog-dependent full-length Gli3 accumulation in primary cilia and
760 subsequent degradation', *Mol Cell Biol*, 30: 1910-22.
761 Zhang, Q., Y. Li, Y. Zhang, V. E. Torres, P. C. Harris, K. Ling, and J. Hu. 2016. 'GTP-binding of
762 ARL-3 is activated by ARL-13 as a GEF and stabilized by UNC-119', *Sci Rep*, 6: 24534.
763 Zugasti, O., J. Rajan, and P. E. Kuwabara. 2005. 'The function and expansion of the Patched-
764 and Hedgehog-related homologs in C. elegans', *Genome Res*, 15: 1402-10.
765

766

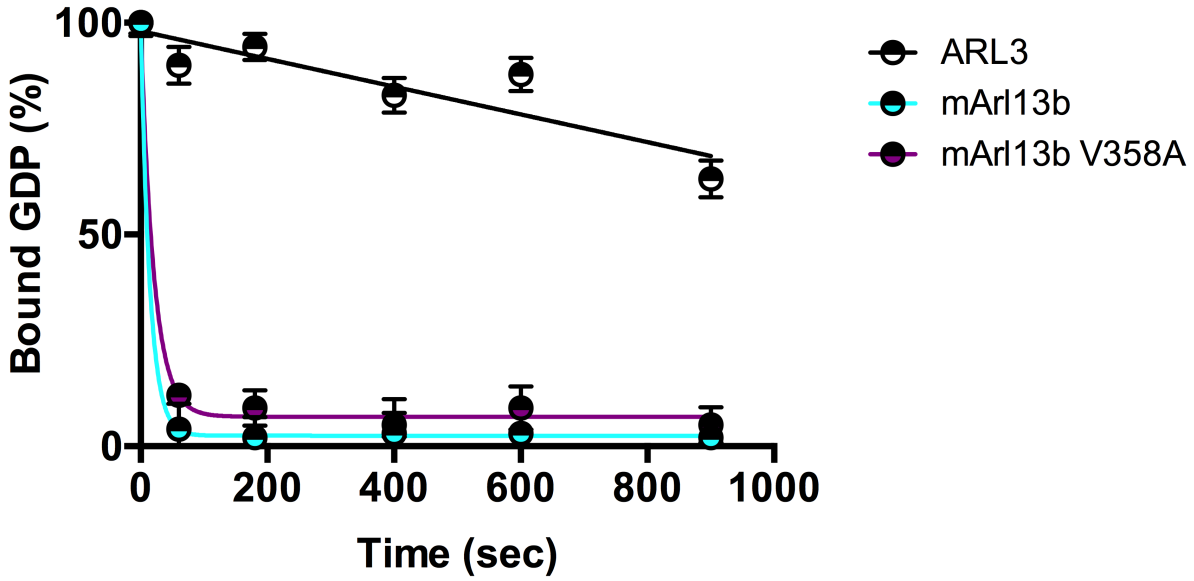

Figure 1.

767 **ARL3 GEF activity is retained in the ARL13B^{V358A} mutant.** Time course of the

768 release of pre-bound [^{3}H]GDP from purified, recombinant ARL3 in the absence (ARL3)

769 or presence of mouse wild type ARL13B or ARL13B^{V358A} (mARL13B) are shown. See

770 Methods for details. Error bars ± standard deviation.

Figure 2.

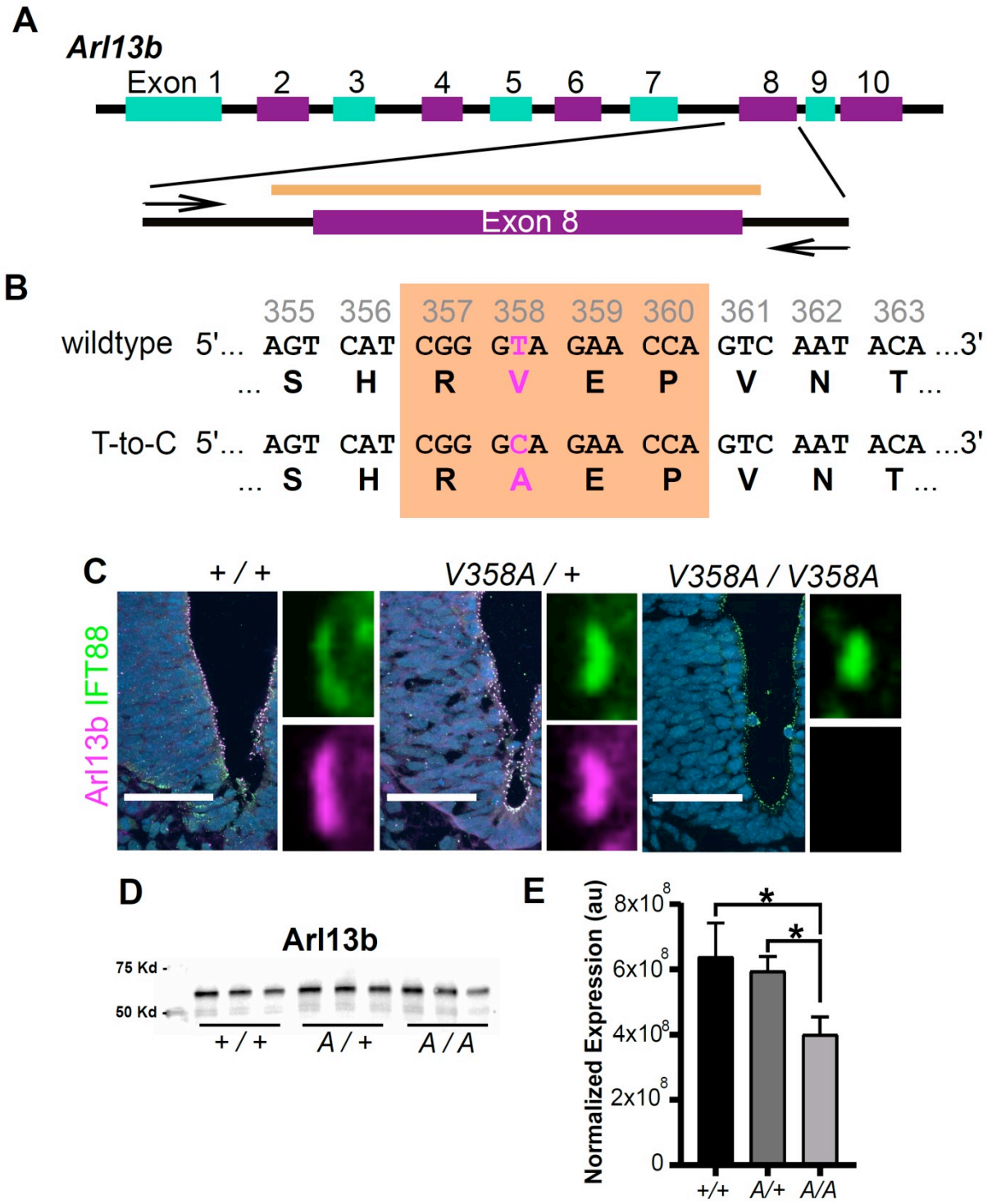
A
Arl13b
Exon 1
2
3
4
5
6
7
8
9
10
Exon 8
B
355 356 357 358 359 360 361 362 363
wildtype 5'... AGT CAT CGG GTA GAA CCA GTC AAT ACA ...3'
... S H R V E P V N T ...
T-to-C 5'... AGT CAT CGG GCA GAA CCA GTC AAT ACA ...3'
... S H R A E P V N T ...
C
+ / +
V358A / +
V358A / V358A
Arl13b IFT88
D
Arl13b
75 Kd
50 Kd
+ / +
A / +
A / A
E
Normalized Expression (au)
8x10^8
6x10^8
4x10^8
2x10^8
0
*
*
+/+
A/+
A/A

Figure 2.

771 **Generation of the *Arl13b*$^{V358A/V358A}$ mouse.**

772 (A) Schematic of *Arl13b* gene and donor oligo (orange bar) at exon 8 used to generate
773 the V358A causing point mutation. Arrows indicate primers used for allele validation. (B)
774 *Arl13b* DNA and relevant amino acid sequence with the RVEP sequence in the orange
775 box and the T-to-C mutation highlighted in pink. (C) Confocal images of cilia marker
776 IFT88 (green) and ARL13B (magenta) staining in neural tube of E10.5 somite-matched
777 embryos. ARL13B-positive cilia are visible in *Arl13b*$^{+/+}$ and *Arl13b*$^{V358A/+}$, but not in
778 *Arl1b*$^{V358A/V358A}$ embryos. At least 5 embryos per genotype across five litters were
779 examined. Scale bars are 50 μm. (D) ARL13B Western blot of E10.5 whole embryo
780 lysates, wild type (+/+), *Arl13b*$^{V358A/+}$ (*A/*+) and *Arl13b*$^{V358A/V358A}$ (*A/A*) and (E)
781 quantification presented as average intensity normalized to total protein ± standard
782 deviation. Representative blot of whole embryo lysates (n = 3 embryos per genotype
783 with technical duplicate of each). * $p < 0.05$, one-way ANOVA and Tukey's multiple
784 comparison.

Figure 3.

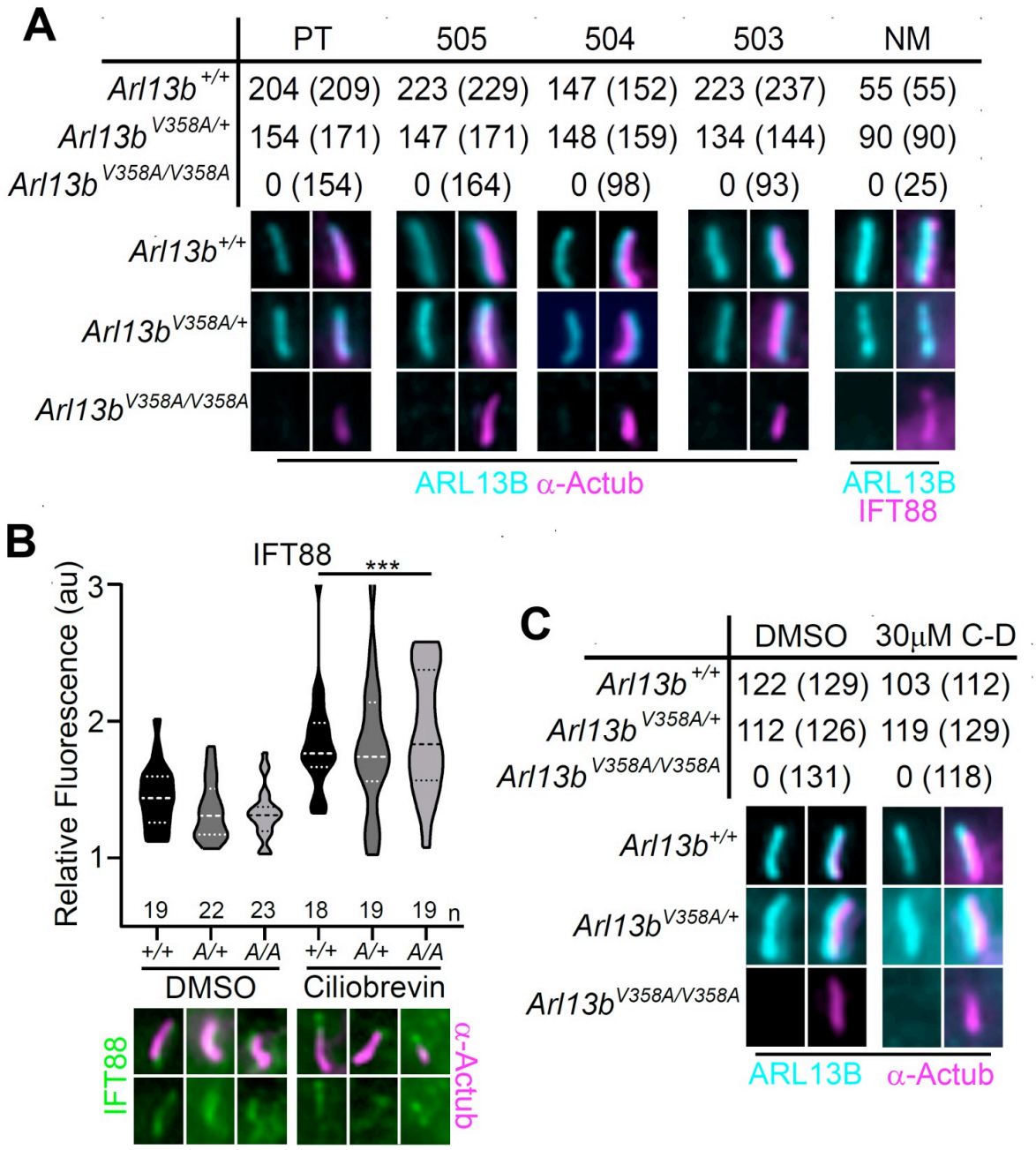
A
PT 505 504 503 NM
Arl13b +/+ 204 (209) 223 (229) 147 (152) 223 (237) 55 (55)
Arl13b V358A/+ 154 (171) 147 (171) 148 (159) 134 (144) 90 (90)
Arl13b V358A/V358A 0 (154) 0 (164) 0 (98) 0 (93) 0 (25)
Arl13b+/+
Arl13bV358A/+
Arl13bV358A/V358A
ARL13B α-Actub
ARL13B
IFT88
B
IFT88
***
Relative Fluorescence (au)
3
2
1
19 22 23 18 19 19 n
+/+ A/+ A/A +/+ A/+ A/A
DMSO
Ciliobrevin
IFT88
α-Actub
C
DMSO 30μM C-D
Arl13b +/+ 122 (129) 103 (112)
Arl13b V358A/+ 112 (126) 119 (129)
Arl13b V358A/V358A 0 (131) 0 (118)
Arl13b+/+
Arl13bV358A/+
Arl13bV358A/V358A
ARL13B α-Actub

Figure 3.

785 **ARL13B^{V358A} is undetectable in cilia and cannot be enriched by inhibition of**
786 **retrograde transport.**

787 (A) Antibodies against ciliary markers acetylated α-tubulin or IFT88 (magenta) and
788 ARL13B (cyan) in *Arl13b*$^{V358A/V358A}$ MEFs. Representative images show staining for five
789 indicated ARL13B antibodies: (PT) polyclonal rabbit antibody against full-length human
790 ARL13B from ProteinTech, (503, 504, 505) polyclonal rabbit sera from three distinct
791 rabbits raised against C-terminus of mouse ARL13B (amino acids 208-427) (Caspary et
792 al. 2007), and (NM) monoclonal mouse antibody against C terminus of mouse ARL13B
793 from NeuroMab. *Arl13b*$^{+/+}$ and *Arl13b*$^{V358A/+}$ show ciliary ARL13B staining. Table lists
794 ARL13B-positive cilia and the total number of cilia identified by acetylated α-tubulin or
795 IFT88 antibody in parentheses. Cilia appear shorter in *Arl13b*$^{V358A/V358A}$ cells (see Fig.
796 6). (B) IFT88 (green) is enriched in the tips of cilia in *Arl13b*$^{+/+}$ (+/+), *Arl13b*$^{V358A/+}$ (*A*/+)
797 and *Arl13b*$^{V358A/V358A}$ (*A/A*) cells following ciliobrevin-D treatment. Violin plots depict
798 relative fluorescence of IFT88 at cilia tip to cell body with number of cilia measured (n)
799 listed beneath each plot. (C) Table lists ARL13B (cyan) positive cilia (rabbit anti-
800 ARL13B; ProteinTech) and the total number of cilia (acetylated α-tubulin: magenta)
801 examined in control (DMSO) and ciliobrevin-D treated (30μM CB) cell lines.
802 Representative images show staining for cilia and ARL13B. Two-way ANOVA and
803 Sidak's multiple comparisons. (*** $p < 0.001$).

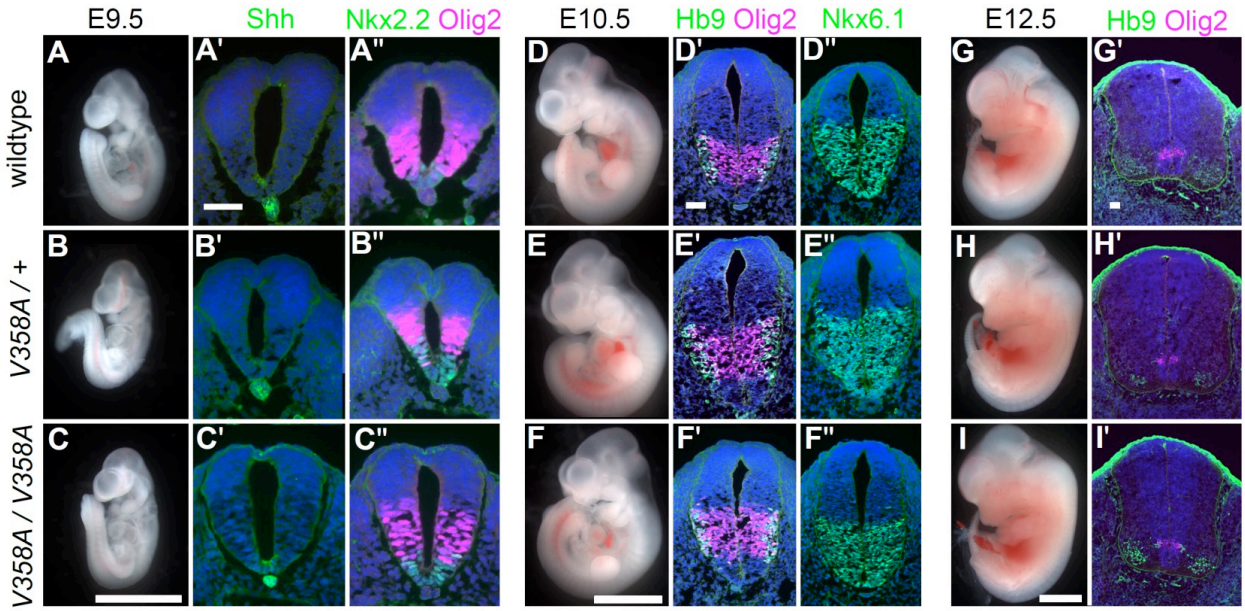

Figure 4.

Arl13b^{V358A} mediates normal Shh signaling and neural tube patterning.

(A-I) Whole embryo and neural tube sections of somite-matched littermates at E9.5, E10.5, and E12.5 stained with indicated markers of cell fate. Whole embryo scale bars: 2 mm. (A'-I' & A"-F") Shh-dependent neural tube patterning at three separate time points. Cell fate markers are listed above each image. All neural tube scale bars are 50 μm. Neural tube patterning was examined in five embryos for each embryonic stage. E, embryonic day.

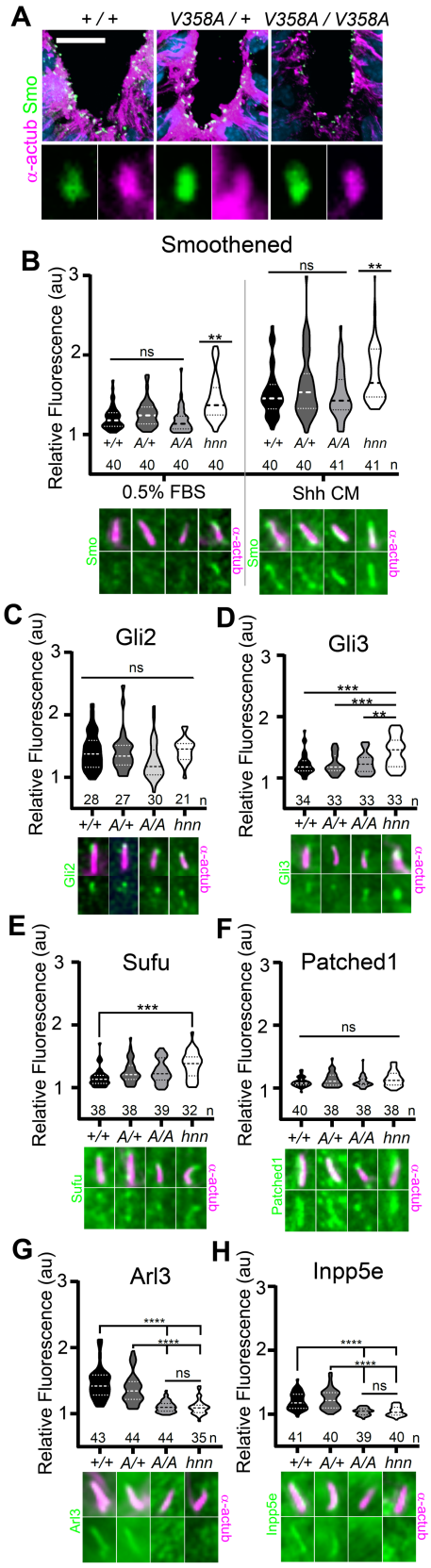
A
+ / +
V358A / +
V358A / V358A
α-actub Smo
B
Smoothened
Relative Fluorescence (au)
ns
**
+/+ A/+ A/A hnn
40 40 40 40
40 40 41 41 n
0.5% FBS
Shh CM
Smo
α-actub
C
Gli2
ns
28 27 30 21 n
D
Gli3
***
**
34 33 33 33 n
E
Sufu
38 38 39 32 n
F
Patched1
40 38 38 38 n
G
Arl3
****
43 44 44 35 n
H
Inpp5e
41 40 39 40 n

Figure 5.

811 **ARL13B^{V358A} mediates normal ciliary enrichment of Shh components, but not**

812 **ARL3 or Inpp5e.**

813 (A) Smo (green) enrichment in ventral neural tube cilia (acetylated α-tubulin: magenta)

814 is normal in E10.5 embryos. Images are confocal projections. Scale bar is 25 μm. (B-H,

815 Top) Quantification of average fluorescence intensity in the tip of the cilium (Gli2, Gli3,

816 and Sufu) or the entire cilium (Ptch1, Smo, ARL3, and Inpp5e) relative to background

817 level. Violin plots depict relative fluorescent intensity per cilium with number of cilia

818 examined below each plot. (B-H, Bottom) Representative images for each condition and

819 cell type with the cilia marker acetylated α-tubulin (magenta) and indicated protein

820 (green). Wild type (+/+), heterozygous (*A/*+), homozygous (*A/A)* and *hennin* (*hnn)*. Data

821 analyzed by one-way ANOVA and Tukey's multiple comparisons, except Smo data

822 analyzed by two-way ANOVA and 16 comparisons, corrected $p < 0.003$ deemed

823 significant. (** $p < 0.01$, *** $p < 0.001$, **** $p < 0.0001$)

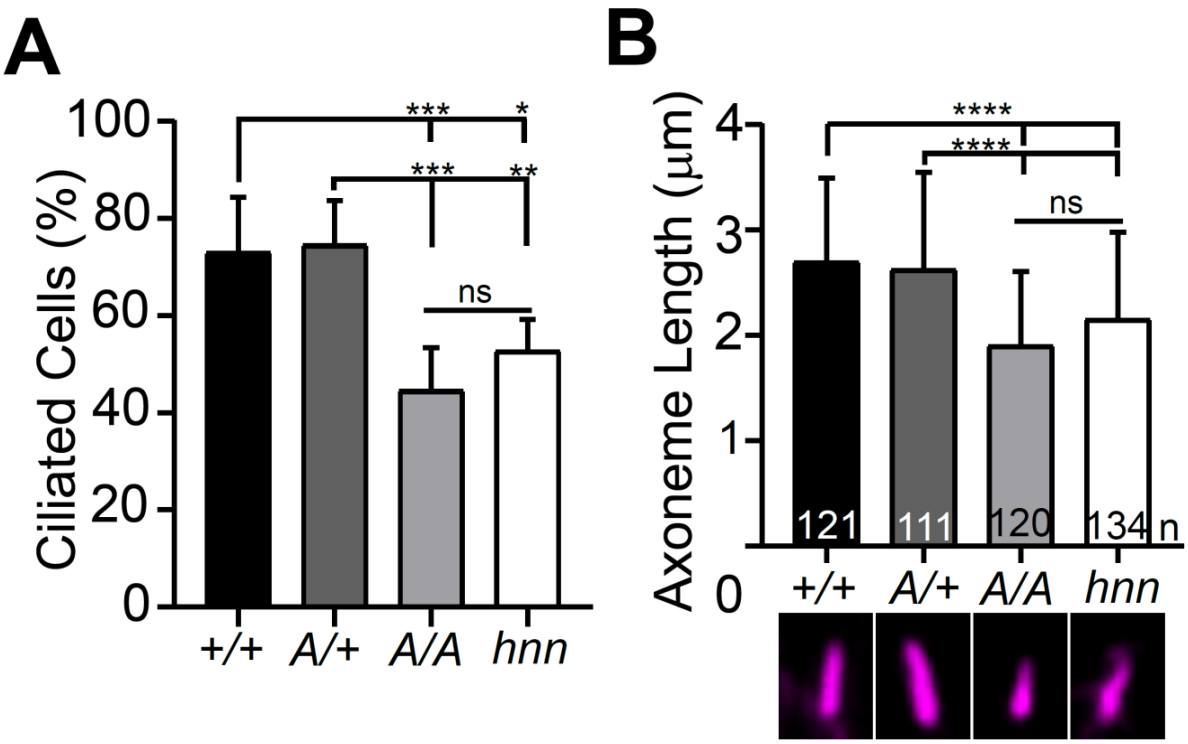

Figure 6.

ARL13B^{V358A} results in decreased ciliation rates and short cilia.

(A) Quantification of ciliation rates in all cell types; wild type (+/+), heterozygous (*A/+*), homozygous (*A/A)* and *hennin* (*hnn)*. Fewer *Arl13b$^{V358A/V358A}$* and *Arl13b$^{hnn/hnn}$* MEFs form cilia compared to *Arl13b$^{+/+}$* or *Arl13b$^{V358A/+}$* cells. (B) Quantification of axoneme length as labeled by acetylated α-tubulin (magenta) in indicated MEFs. Data are presented as mean (μm) ± standard deviation with the number of cilia measured per genotype depicted at the base of each bar. Data analyzed by one-way ANOVA and Tukey's multiple comparisons. (* $p < 0.05$, ** $p < 0.01$, *** $p < 0.001$, **** $p < 0.0001$)

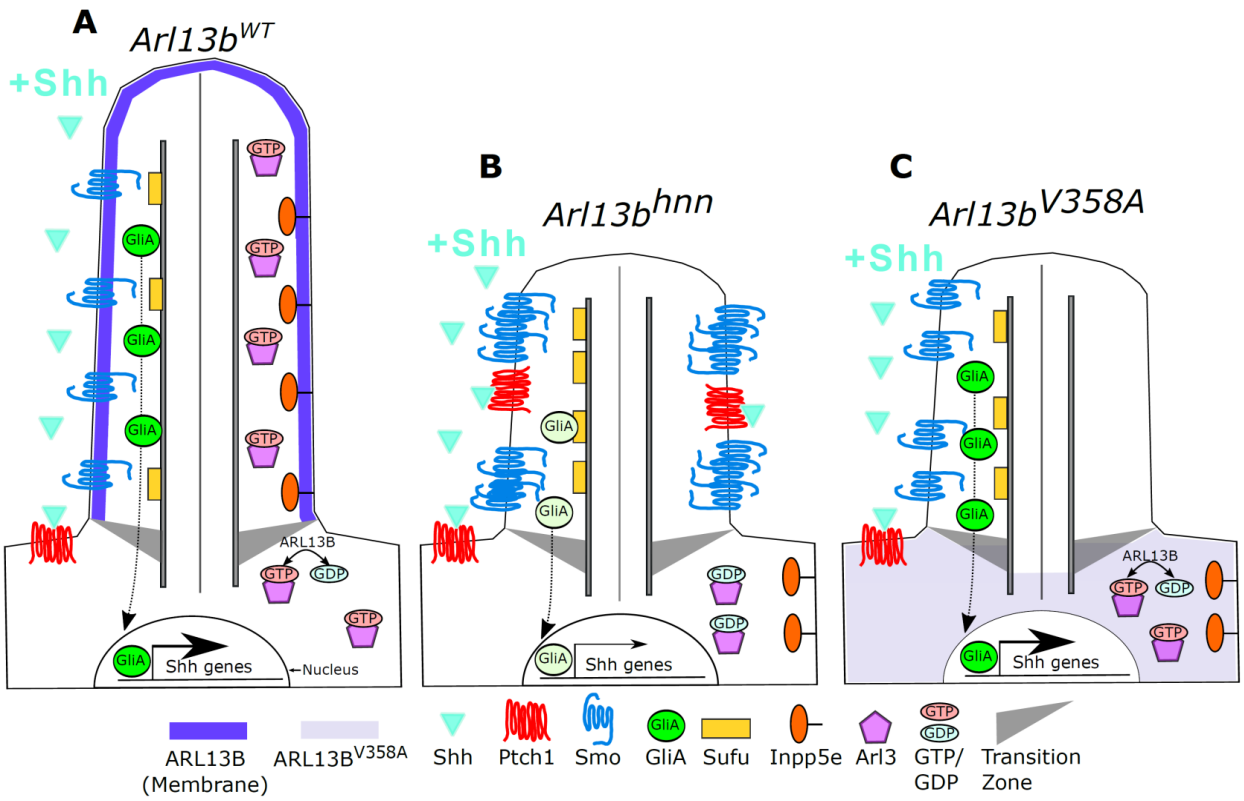

Figure 7.

Model comparing complete loss of ARL13B function to ciliary loss of ARL13B function

Wildtype (left), *Arl13b*^{hnnhnn} (middle), and *Arl13b*$^{V358A/V358A}$ (right) cilia represented as two halves. On the left half is the organization of Shh components in the presence of Shh ligand and on the right half is the organization of ARL13B interactors ARL3 and Inpp5e. (A) ARL13B associates with the ciliary membrane. In the presence of Shh, Ptch1 is removed from cilia and Smo is visibly enriched in cilia. Smo is activated which promotes the processing of full-length Gli transcription factors into their activator forms (GliA), that are shuttled out of the cilium to promote Shh-dependent gene transcription. In addition, cilia proteins ARL3 and Inpp5e are localized to the primary cilium. (B) In *Arl13b*$^{hnn/hnn}$ cells which are null for ARL13B, cilia are shorter than normal. Ciliary Ptch1 and Smo are

843 visible, although Smo appears punctate instead of diffuse. In addition, loss of ARL13B
844 decreases transcription of Shh-dependent genes due to lowered GliA. *Arl13b*$^{hnn/hnn}$ cilia
845 also display a failure of Inpp5e and ARL3 to localize to the cilium. Because ARL13B is
846 the GEF for ARL3, we speculate in this schematic that ARL3 remains GDP bound in
847 *Arl13b*$^{hnn/hnn}$ cells. (C) In *Arl13b*$^{V358A/V358A}$ cells, ARL13B^{V358A} is not detectable in cilia
848 and appears diffuse within the cell body. *Arl13b*$^{V358A/V358A}$ cilia, like *Arl13b*$^{hnn/hnn}$ cilia, are
849 shorter than wildtype. We observe normal Shh-dependent ciliary Smo enrichment and
850 normal Shh transcriptional output. However, ARL3 and Inpp5e are absent from cilia,
851 indicating that ciliary ARL13B is required for ciliary residence of these proteins.

MICE	Sex	wildtype	*V358A/+*	*V358A/V358A*	
Het x Het	M (46.5%)	3	11	6	
Avg. Litter	F (53.5%)	6	8	9	
7.3	% of Total	20.9	44.2	34.9	$\chi^2 = 0.60$
Het x Hom	M (60%)	-	10	11	
Avg. Litter	F (40%)	-	6	8	
7.5	% of Total	-	45.7	54.3	$\chi^2 = 0.69$
Hom x Hom	M (47.4%)	-	-	9	
Avg. Litter	F (52.6%)	-	-	10	
9.5					

Table 1.

852 Genotype of mice born to heterozygous and/or homozygous carrier parents. Data

853 analyzed by chi-squared test.

Supplemental Figure 1.

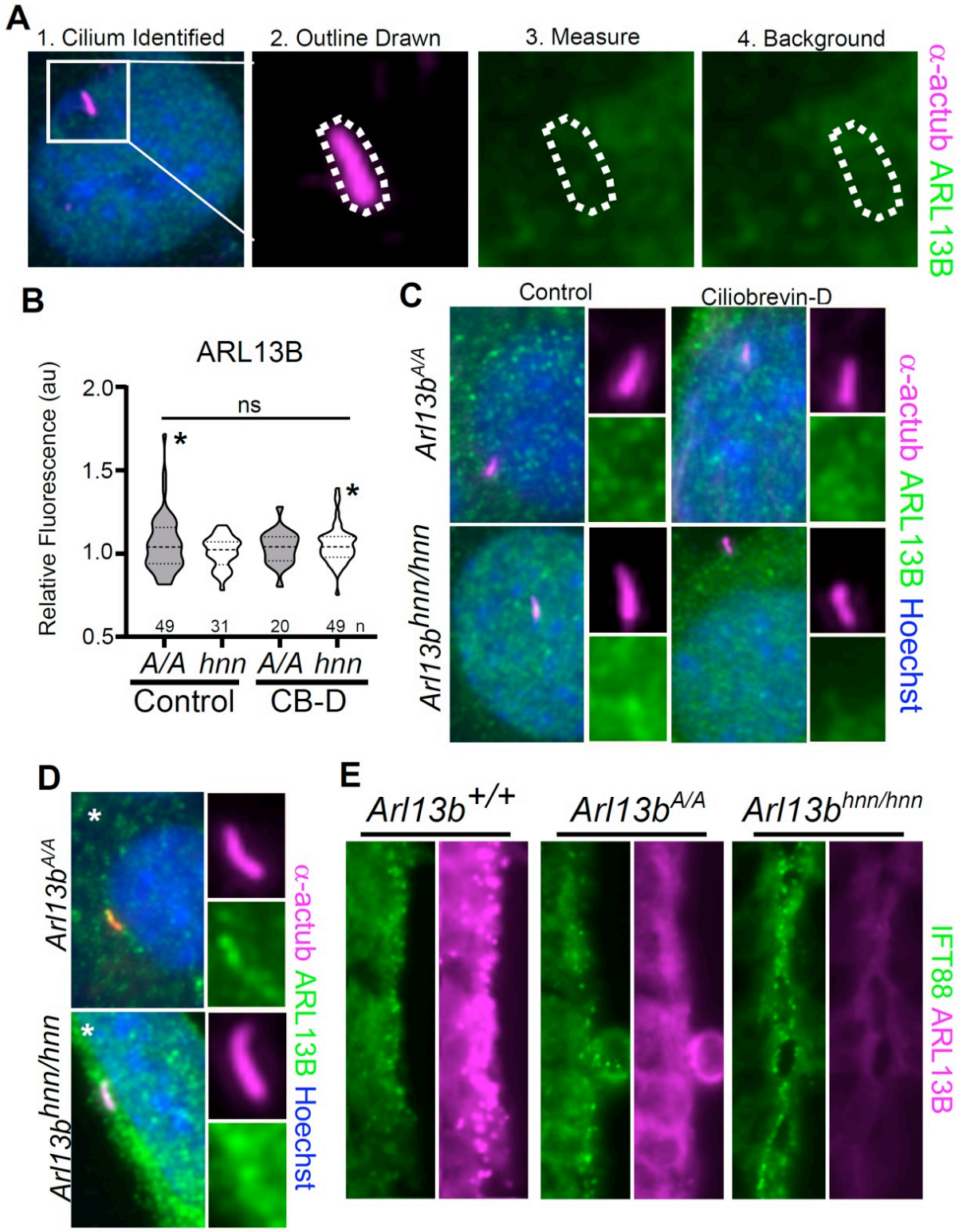

Supplemental Figure 1.

854 **Overexposure of *Arl13b*$^{V358A/V358A}$ cilia in E10.5 neural tube and MEFs reveals no**
855 **clear ARL13B^{V358A} presence in cilia.**

856 (A) We identified acetylated α-tubulin positive cilia and used the marker to outline the
857 area of the cilium. We quantified ARL13B immunofluorescence detected by Caspary lab
858 polyclonal anti-ARL13B antibody (Caspary et al. 2007) and used the same trace to
859 measure background levels in a different area of the cell body. (B) *Arl13b*$^{V358A/V358A}$
860 (*A/A*) and *Arl13b*$^{hnn/hnn}$ (*hnn*) MEFs treated with control or ciliobrevin-D 0.5% FBS
861 Media. Samples were overexposed five times longer than normal, saturating the
862 detector in the ARL13B channel. We measured no difference in ciliary ARL13B
863 immunofluorescence between control and ciliobrevin-D treated *Arl13b*$^{V358A/V358A}$ and
864 *Arl13b*$^{hnn/hnn}$ MEFs. Data presented as violin plots and analyzed by one-way ANOVA.
865 Respective number of cilia listed below each plot. Cilia that had ARL13B
866 immunofluorescent readings above background (*) are shown in panel D. (C)
867 Representative images of over exposed *Arl13b*$^{V358A/V358A}$ and *Arl13b*$^{hnn/hnn}$ MEFs in
868 control and ciliobrevin-D treatment conditions. (D) Representative images of cilia with
869 ARL13B levels above background, marked by * in panel B. (E) Overexposure of cilia in
870 E10.5 *Arl13b*$^{+/+}$, *Arl13b*$^{V358A/V358A}$, and *Arl13b*$^{hnn/hnn}$ embryonic neural tube, stained for
871 IFT88 and ARL13B (NeuroMab). The ARL13B channel was overexposed for four
872 seconds instead of one second.